ECCOMAS Congress 2016
VII European Congress on Computational Methods in Applied Sciences and Engineering
M. Papadrakakis, V. Papadopoulos, G. Stefanou, V. Plevris (eds.)
Crete Island, Greece, 5–10 June 2016

ENERGY CONSERVING TIME INTEGRATION BASED ON GALERKIN-VARIATIONAL INTEGRATORS WITH CONSTRAINTS

Matthias Bartelt[1] **and Michael Groß**[2]

Technische Universität Chemnitz, Professorship of applied mechanics and dynamics
Reichenhainer Straße 70, D-09126 Chemnitz
[1] e-mail: matthias.bartelt@mb.tu-chemnitz.de [2] e-mail: michael.gross@mb.tu-chemnitz.de

Keywords: Variational integrator, energy conservation, finite element method, higher-order time integration, Lagrange multiplier method

Abstract. *Often, Lagrange's formalism based on the Lagrangian is the preferred way in order to derive equations of motion for a mechanical system. Therefore, the first step is the formulation of the total kinetic and total potential energy. In this formalism, holonomic constraints can be taken into account by using the Lagrange multiplier method, and external and dissipative forces can be included variationally consistently by means of the Lagrange-D'Alembert principle. In this way, we are directly arrive at a weak formulation of the equations of motion without using a strong form and integration by parts. The variational time integration method is now based on the discretization of the action functional and the discrete variational calculus. This method leads to time stepping schemes called variational integrators.*
In this paper, we show that variational integrators based on higher-order shape functions and quadrature rules leads to a higher-order time approximation, which preserve the total linear and total angular momentum of the mechanical system. A further topic of the paper is a new implementation of the Lagrange multiplier method for holonomic constraints in the higher-order variational integrator, in order to compute bearing forces by means of Lagrange multipliers.
Usually, variational integrators show an excellent long time behavior and bind the total energy error per time step, but are not able to preserve the total energy exactly. Therefore, we introduce a discrete gradient of the total potential energy in the variational integrator to preserve the total energy. We show different discrete gradients with different results for numerical stability. We can show that these time stepping schemes preserve the total linear momentum, total angular momentum as well as the total energy for every time step size.
As numerical examples, we show motions of three-dimensional continua, which are discretized in space by the finite element method. We start with a free flying hyper-elastic rotor to show the preservation of total linear and total angular momentum in combination with higher-order accuracy in time. In the second example, we consider a hyper-elastic beam and apply the Lagrange multiplier method in order to calculate the bearing forces at fixed nodes. In the last example, the energy conservation is shown for different discrete gradients.

1 INTRODUCTION

This paper shows the application of a variational formulation in time to create an *energy-conserving* variational integrator of higher order accuracy for finite element models. A three-dimensional body will be discretized with linear finite elements in space. We also apply DIRICHLET boundaries and show how these can be included in the variational principle. For this, we use LAGRANGE multiplier with a special NEWTON-COTÊS approximation. The calculation of the bearing forces will be described, which is needed for the calculation of the balance of total angular momentum. A *standard* variational integrator is total linear and total angular momentum conserving, however does not preserve the total energy of a discrete conservative system. But, the introduction of the enhanced derivative or gradient, respectively, in Reference [1] in the variational integrator leads to a variational based time integration algorithm, which preserves the discrete balance of total energy.

First of all, the introduction of the enhanced gradient is consistent with the LAGRANGE-D'ALEMBERT principle and therefore generates an extended variational integrator. This knowledge can be derived from the generalization of the discrete derivative or gradient, respectively, in Reference [8] to higher order schemes [1]. For higher order schemes, the discrete gradient of the total energy is always split into two terms of a sum. The first term is a conservative part, which arises in a variational integrator from the discretized Lagrangian of the dynamical system. The second term as extension of the conservative part can be considered as a special non-conservative extension of the dynamical system. The special feature of this term is, that it does not lead to a physically based energy dissipation or a physically based external work, but rather to an algorithmic energy conservation in the discrete variational system and to a zero term in the continuous variational system. In Reference [1] is also shown, that both parts can be derived from a separate constraint variational problem, which can be concatenated with the variational formulation of the dynamical system.

Another interesting point of view is to recognize in the second term of the enhanced gradient an energy error controller. In Reference [11], there is described a so-called *affine Hamiltonian control system* with an extended Hamiltonian

$$H(\mathbf{q},\mathbf{p},\mathbf{u}) = H_0(\mathbf{q},\mathbf{p}) - \sum_{j=1}^{n_{\mathrm{con}}} H_j(\mathbf{q},\mathbf{p})\, u_j \tag{1}$$

which depends only linearly or affine on the control variables u_j, $j = 1,\ldots,n_{\mathrm{con}}$. The function H_0 is called the internal Hamiltonian of the dynamical system, and the functions H_j are called coupling Hamiltonians. Accordingly, the natural outputs y_j, $j = 1,\ldots,n_{\mathrm{con}}$ of the Hamiltonian system are given by

$$y_j = \frac{\partial H}{\partial u_j} \tag{2}$$

Taking into account Hamilton's principle, we arrive in the continuous setting at the affine Hamiltonian control system

$$\dot{\mathbf{q}} = \frac{\partial H_0}{\partial \mathbf{p}} - \sum_{j=1}^{n_{\mathrm{con}}} \frac{\partial H_j}{\partial \mathbf{p}}\, u_j \tag{3}$$

$$\dot{\mathbf{p}} = -\frac{\partial H_0}{\partial \mathbf{q}} + \sum_{j=1}^{n_{\mathrm{con}}} \frac{\partial H_j}{\partial \mathbf{q}}\, u_j \tag{4}$$

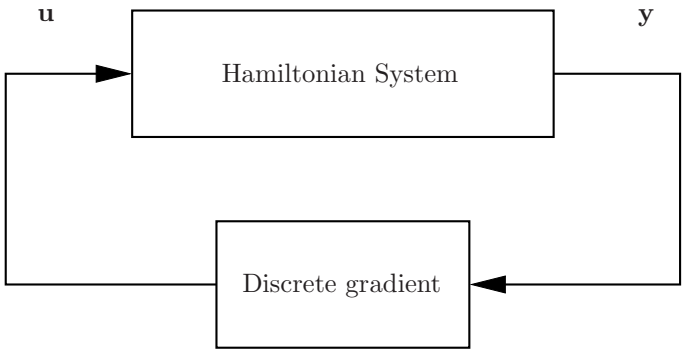

Figure 1: Discrete gradient as energy error controller of a time integrator

with the corresponding total energy balance

$$\frac{\mathrm{d}H_0}{\mathrm{d}t} = \sum_{j=1}^{n_{\mathrm{con}}} \dot{y}_j \, u_j \tag{5}$$

Hence, in the continuous setting the input variables have to vanish for total energy conservation, but in the discrete setting the sum balance the energy error of the time integrator. Comparing this Hamiltonian formulation with that in Reference [1], it is obvious that the control inputs u_j are the components of the second term of the enhanced gradient, following from a costoptimized constraint optimization problem and leading to an energy consistent algorithmic *closed loop control problem*.

Consequently, the enhanced gradient as higher order accurate discrete gradient can be seen at least in two ways as a consistent extension of a variational based time integrator. In this work, the first method of using the LAGRANGE-D'ALEMBERT principle is shown in a continuous as well as discrete setting.

2 FINITE ELEMENT APPROXIMATION

We choose a standard spatial finite element discretization for the solid continuum. First we define a model in the reference configuration $\mathcal{B}_0$ at time $t = 0$. The deformed model is denoted by the configurations $\mathcal{B}_t$ for $t > 0$. The postion vector in configuration $\mathcal{B}_0$ is described by the vector $\mathbf{X} \in \mathbb{R}^n$. For the configuration $\mathcal{B}_t$, the new position vector depends on time t with $\mathbf{x}(t) \in \mathbb{R}^n$. The index n means the number of degrees of freedom for the three-dimensional discretized continuum.

$$\mathbf{X} \in \mathbb{R}^n \text{ in } \mathcal{B}_0 \text{ and } \mathbf{x}(t) \in \mathbb{R}^n \text{ in } \mathcal{B}_t \tag{6}$$

With an application of the isoparametric concept [3], we define a function $\boldsymbol{\varphi}$. This makes it possible to calculate the actual postion from the reference configuration and the actual time t. The actual position depends on a linear mapping

$$\mathbf{x}(t) = \boldsymbol{\varphi}(\mathbf{X}, t). \tag{7}$$

The position vectors are approximated in space with linear LAGRANGE-polynomials N^A on the reference element with coordination vector $\boldsymbol{\xi}$. This finite element is also known as C3D8 cube.

$$\mathbf{X}^{e,\mathrm{h}} = \sum_{A=1}^{n_{\mathrm{s}}} N^A(\boldsymbol{\xi}) \mathbf{X}^{e,A} \tag{8}$$

$$\mathbf{x}^{e,\mathrm{h}} = \sum_{A=1}^{n_\mathrm{s}} N^A(\boldsymbol{\xi})\mathbf{q}^{e,A} \tag{9}$$

The deformation gradient is defined by the derivative of the function $\boldsymbol{\varphi}$ with respect to $\mathbf{X}$,

$$\mathbf{F}(\mathbf{X},t) = \nabla_{\mathbf{X}}\boldsymbol{\varphi}(\mathbf{X},t) \tag{10}$$

with

$$\mathbf{F}^e = \sum_{A=1}^{n_\mathrm{s}} \mathbf{q}^{e,A} \otimes \left((\mathbf{J}^e)^{-\mathrm{T}} \cdot \frac{\partial N^A(\boldsymbol{\xi})}{\partial \boldsymbol{\xi}} \right). \tag{11}$$

and

$$\mathbf{J}^e = \sum_{A=1}^{n_\mathrm{s}} \mathbf{X}^{e,A} \otimes \frac{\partial N^A(\boldsymbol{\xi})}{\partial \boldsymbol{\xi}} \tag{12}$$

The deformation gradient $\mathbf{F}$ provides a relationship between tangent vectors in the reference and actual configuration of a continuum. For the description of the deformation measurement we choose the right-CAUCHY-GREEN tensor

$$\mathbf{C} = \mathbf{F}^{\mathrm{T}}\mathbf{F} \tag{13}$$

The third invariant of $\mathbf{F}$ can also be defined in $\mathbf{C}$ as

$$I_3(\mathbf{F}) = \sqrt{\det(\mathbf{C})}. \tag{14}$$

We also define the derivative of the tensor $\mathbf{C}$ with respect to $\mathbf{q}$ as the linearized strain operator

$$\mathbb{B}^{e,A} = 2\frac{\partial \mathbf{C}^e}{\partial \mathbf{q}^e} = 2\nabla_{\mathbf{X}} N^A \otimes \mathbf{F}^{e^{\mathrm{T}}}. \tag{15}$$

2.1 MATERIAL FORMULATION

The used material model is described by the following free energy function see also [5] and [10].

$$\psi = \frac{\mu}{2}\left[\mathrm{tr}(\mathbf{C}) - n_{\mathrm{dim}} - 2\ln(I_3(\mathbf{C}))\right] + \psi^{\mathrm{vol}} \tag{16}$$

$$\psi^{\mathrm{vol}} = \frac{\lambda}{2}\left[\ln(I_3(\mathbf{C}))^2 + (I_3(\mathbf{C}) - 1)^2\right] \tag{17}$$

The constants λ and μ are called LAMÉ-parameters. In the three-dimensional case, n_{dim} is set to three. This matrial model, in combination with the formulation of the right-CAUCHY-GREEN tensor, allows us to decribe large deformations for the physical model.

3 THE LAGRANGIAN

The LAGRANGE function, defined by the kinetic energy T^{kin} and potential energy V^{int}, is given by

$$\mathcal{L} = T^{\mathrm{kin}} - V^{\mathrm{int}} \tag{18}$$

As potential energy $V^{\text{int},e}$, we define the integral over free energy function ψ^e for every element and the gravity with respect to the reference configuration $\mathcal{B}_0$. The kinetic energy $T^{\text{kin},e}$ for one element depends on the mass matrix $\mathbb{M}^e$ and the velocity $\dot{\mathbf{q}}^e$.

$$V^{\text{int},e} = \int_{\mathcal{B}_0^e} \rho_0 \psi^e(\mathbf{C}^e(\mathbf{q}^e)) + \rho_0 \mathbf{g}^e \cdot \mathbf{q}^e \mathrm{d}V \tag{19}$$

$$T^{\text{kin}} = \frac{1}{2} \int_{\mathcal{B}_0^e} \rho_0 \dot{\mathbf{q}} \cdot \dot{\mathbf{q}} \tag{20}$$

$$T^{\text{kin},e} = \frac{1}{2} \dot{\mathbf{q}}^e \cdot \mathbb{M}^e \cdot \dot{\mathbf{q}}^e \tag{21}$$

The gravitational vector $\mathbf{g}^e$ is defined by $\mathbf{g}^e = g[0, -e_y, 0]^{\mathrm{T}}$ with g as the gravitational constant.

3.1 APPROXIMATION IN TIME

The postion vector $\mathbf{q}$ and velocity vector $\dot{\mathbf{q}}$ are discretized in the following way:

$$\mathbf{q}^{\mathrm{h}} = \sum_{i=0}^{n_{\mathrm{p}}} M_i(\alpha) \mathbf{q}_{\frac{i}{n_{\mathrm{p}}}} \qquad \mathbf{q}^{\mathrm{d}} = \sum_{i=0}^{n_{\mathrm{p}}} M_i^{'}(\alpha) \mathbf{q}_{\frac{i}{n_{\mathrm{p}}}} \qquad i = 0 \ldots n_{\mathrm{p}} \tag{22}$$

n_{p} is the number of polynomial degree and M represents the LAGRANGE polynomials in the interval from zero to one. For this approximation, we need specific quadrature points $\alpha_j, j = 1, \ldots, n_{\mathrm{q}}$. In this paper, we only use GAUSSIAN quadrature points and LAGRANGE polynomials with equidistant points in the interval from zero to one. Note that, it is also possible to choose other quadrature points or other shape functions in time. The approximated velocity vector $\dot{\mathbf{q}}$ is defined by the derivative of the position vector with respect to the time t. This derivative will be replaced by a derivative of $M(\alpha)$ with respect to α.

$$\dot{\mathbf{q}}(t) = \sum_{i=0}^{n_{\mathrm{p}}} \frac{\mathrm{d}M(\alpha(t))}{\mathrm{d}t} \mathbf{q}_{\frac{i}{n_{\mathrm{p}}}} = \sum_{i=0}^{n_{\mathrm{p}}} \frac{1}{h_n} \frac{\partial M(\alpha)}{\partial \alpha} \mathbf{q}_{\frac{i}{n_{\mathrm{p}}}} = \sum_{i=0}^{n_{\mathrm{p}}} \frac{1}{h_n} M_i^{'}(\alpha) \mathbf{q}_{\frac{i}{n_{\mathrm{p}}}} = \frac{1}{h_n} \mathbf{q}^{\mathrm{d}} \tag{23}$$

3.2 THE DISCRETE STATE SPACE DEFINITION

We divide one time interval with the size h_n into different micro time steps. The number of micro time steps depends on the polynomial degree of approximation in time. This will be applied to the position vector $\bar{\mathbf{q}}_{k+1}$ and the LAGRANGE-multiplier vector $\bar{\boldsymbol{\lambda}}_{k+1}$.

$$\bar{\mathbf{q}}_{k+1} = \left[\mathbf{q}_k, \mathbf{q}_{k+\frac{1}{n_{\mathrm{p}}}}, \mathbf{q}_{k+\frac{2}{n_{\mathrm{p}}}}, \ldots, \mathbf{q}_{k+\frac{n_{\mathrm{p}}-1}{n_{\mathrm{p}}}}, \mathbf{q}_{k+1} \right]^{\mathrm{T}} \tag{24}$$

$$\bar{\boldsymbol{\lambda}}_{k+1} = \left[\boldsymbol{\lambda}_k, \boldsymbol{\lambda}_{k+\frac{1}{n_{\mathrm{p}}}}, \boldsymbol{\lambda}_{k+\frac{2}{n_{\mathrm{p}}}}, \ldots, \boldsymbol{\lambda}_{k+\frac{n_{\mathrm{p}}-1}{n_{\mathrm{p}}}}, \boldsymbol{\lambda}_{k+1} \right]^{\mathrm{T}}$$

The total number of all state variables is summarized in $\bar{\mathbf{q}}^{\text{tot}}$ and $\bar{\boldsymbol{\lambda}}^{\text{tot}}$. The number of all macro time steps is equal to n_{t}.

$$\bar{\mathbf{q}}^{\text{tot}} = \left[\mathbf{q}_{0+\frac{0}{n_{\mathrm{p}}}}, \mathbf{q}_{0+\frac{1}{n_{\mathrm{p}}}}, \mathbf{q}_{0+\frac{2}{n_{\mathrm{p}}}}, \ldots, \mathbf{q}_{0+\frac{n_{\mathrm{p}}-1}{n_{\mathrm{p}}}}, \mathbf{q}_{1+\frac{0}{n_{\mathrm{p}}}}, \ldots, \mathbf{q}_{n_{\mathrm{t}}-1+\frac{n_{\mathrm{p}}-1}{n_{\mathrm{p}}}}, \mathbf{q}_{n_{\mathrm{t}}} \right]^{\mathrm{T}} \tag{25}$$

$$\bar{\boldsymbol{\lambda}}^{\text{tot}} = \left[\boldsymbol{\lambda}_{0+\frac{0}{n_{\mathrm{p}}}}, \boldsymbol{\lambda}_{0+\frac{1}{n_{\mathrm{p}}}}, \boldsymbol{\lambda}_{0+\frac{2}{n_{\mathrm{p}}}}, \ldots, \boldsymbol{\lambda}_{0+\frac{n_{\mathrm{p}}-1}{n_{\mathrm{p}}}}, \boldsymbol{\lambda}_{1+\frac{0}{n_{\mathrm{p}}}}, \ldots, \boldsymbol{\lambda}_{n_{\mathrm{t}}-1+\frac{n_{\mathrm{p}}-1}{n_{\mathrm{p}}}}, \boldsymbol{\lambda}_{n_{\mathrm{t}}} \right]^{\mathrm{T}}$$

The continuous LAGRANGIAN will be approximated with discretized variables, see below.

3.3 THE DISCRETE LAGRANGIAN

$$\tilde{\mathcal{L}}_{\mathrm{d}} = \int_{t_k}^{t_{k+1}} \frac{1}{2}\dot{\mathbf{q}}^{\mathrm{h}} \cdot \mathbb{M} \cdot \dot{\mathbf{q}}^{\mathrm{h}} \mathrm{d}t - \int_{t_k}^{t_{k+1}} \int_{\mathcal{B}_0} \rho_0 \psi(\mathbf{C}(\mathbf{q}^{\mathrm{h}})) + \rho_0 \mathbf{g} \cdot \mathbf{q}^{\mathrm{h}} \mathrm{d}V \mathrm{d}t - \int_{t_k}^{t_{k+1}} \boldsymbol{\lambda} \cdot \boldsymbol{\Phi}\left(\mathbf{q}\right) \mathrm{d}t \tag{26}$$

First we define a discrete functional $\mathcal{L}_{\mathrm{d},k+1}$ without the LAGRANGE multiplier vector $\boldsymbol{\lambda}$.

$$\mathcal{L}_{\mathrm{d},k+1}(\bar{\mathbf{q}}_{k+1}) = h_n \sum_{m=1}^{n_{\mathrm{q}}} w_m \mathcal{L}(\mathbf{q}_{k+1}, \dot{\mathbf{q}}_{k+1}) \tag{27}$$

The reason is, we want to fulfill constraints at the micro time steps and not at the quadrature points. Therefore we apply a NEWTON-COTÊS quadrature for the constraint terms. The application of the NEWTON-COTÊS quadrature, with an equidistant choice of quadrature points, decouples the following equations and defines the LAGRANGE multiplier at the micro time steps.

$$\tilde{\mathcal{L}}_{\mathrm{d},k+1}(\bar{\mathbf{q}}_{k+1}, \bar{\boldsymbol{\lambda}}_{k+1}) = \mathcal{L}_{\mathrm{d},k+1}(\bar{\mathbf{q}}_{k+1}) - h_n \sum_{i=0}^{n_{\mathrm{q}}} w_{\mathrm{c}} M_{\mathrm{c},i}(\alpha_{\mathrm{c}}) \tilde{\boldsymbol{\lambda}}_{k+\frac{i}{n_{\mathrm{p}}}} \cdot \boldsymbol{\Phi}\left(\mathbf{q}_{k+\frac{i}{n_{\mathrm{p}}}}\right) \tag{28}$$

The shape functions in time for the NEWTON-COTÊS quadrature are always one for the quadrature points and zero for all other shape functions.

$$\sum_{i=0}^{n_{\mathrm{q}}} w_{\mathrm{c}} M_{\mathrm{c},i}(\alpha_{\mathrm{c}}) \tilde{\boldsymbol{\lambda}}_{k+\frac{i}{n_{\mathrm{p}}}} = \sum_{i=0}^{n_{\mathrm{q}}} w_{\mathrm{c}} \tilde{\boldsymbol{\lambda}}_{k+\frac{i}{n_{\mathrm{p}}}} \tag{29}$$

We also define a new LAGRANGE multiplier vector $\boldsymbol{\lambda}_{k+\frac{i}{n_{\mathrm{p}}}}$ which includes the weight from the quadrature.

$$\tilde{\mathcal{L}}_{\mathrm{d},k+1}(\bar{\mathbf{q}}_{k+1}, \bar{\boldsymbol{\lambda}}_{k+1}) = \mathcal{L}_{\mathrm{d},k+1}(\bar{\mathbf{q}}_{k+1}) - h_n \sum_{i=0}^{n_{\mathrm{q}}} \boldsymbol{\lambda}_{k+\frac{i}{n_{\mathrm{p}}}} \cdot \boldsymbol{\Phi}\left(\mathbf{q}_{k+\frac{i}{n_{\mathrm{p}}}}\right) \tag{30}$$

We build the discrete action sum $\mathcal{S}_{\mathrm{d}}$ as a sum over all time steps.

$$\begin{aligned} \delta \mathcal{S}_{\mathrm{d}} &= \delta \sum_{k=0}^{n_{\mathrm{t}}-1} \tilde{\mathcal{L}}_{\mathrm{d},k+1} \\ &= \frac{\partial}{\partial \bar{\mathbf{q}}^{\mathrm{tot}}} \left(\sum_{k=0}^{n_{\mathrm{t}}-1} \tilde{\mathcal{L}}_{\mathrm{d},k+1} \right) \cdot \delta \bar{\mathbf{q}}^{\mathrm{tot}} + \frac{\partial}{\partial \bar{\boldsymbol{\lambda}}^{\mathrm{tot}}} \left(\sum_{k=0}^{n_{\mathrm{t}}-1} \tilde{\mathcal{L}}_{\mathrm{d},k+1} \right) \cdot \delta \bar{\boldsymbol{\lambda}}^{\mathrm{tot}} \end{aligned} \tag{31}$$

The first variation with respect to $\bar{\mathbf{q}}^{\mathrm{tot}}$ gives us:

$$\begin{aligned} &\frac{\partial}{\partial \bar{\mathbf{q}}^{\mathrm{tot}}} \left(\sum_{k=0}^{n_{\mathrm{t}}-1} \tilde{\mathcal{L}}_{\mathrm{d},k+1} \right) \cdot \delta \bar{\mathbf{q}}^{\mathrm{tot}} \\ &= \sum_{k=0}^{n_{\mathrm{t}}-1} \left[\mathrm{D}_1 \tilde{\mathcal{L}}_{\mathrm{d},k+1} \cdot \delta \mathbf{q}_k + \sum_{i=1}^{n_{\mathrm{p}}-1} \left(\mathrm{D}_{1+i} \tilde{\mathcal{L}}_{\mathrm{d},k+1} \cdot \delta \mathbf{q}_{k+\frac{i}{n_{\mathrm{p}}}} \right) + \mathrm{D}_{1+n_{\mathrm{p}}} \tilde{\mathcal{L}}_{\mathrm{d},k+1} \cdot \delta \mathbf{q}_{k+1} \right] \\ &= \sum_{k=0}^{n_{\mathrm{t}}-1} \sum_{i=1}^{n_{\mathrm{p}}-1} \left(\mathrm{D}_{1+i} \tilde{\mathcal{L}}_{\mathrm{d},k+1} \cdot \delta \mathbf{q}_{k+\frac{i}{n_{\mathrm{p}}}} \right) + \sum_{k=1}^{n_{\mathrm{t}}-1} \left(\mathrm{D}_1 \tilde{\mathcal{L}}_{\mathrm{d},k+1} + \mathrm{D}_{1+n_{\mathrm{p}}} \tilde{\mathcal{L}}_{\mathrm{d},k} \right) \cdot \delta \mathbf{q}_k \\ &+ \mathrm{D}_1 \tilde{\mathcal{L}}_{\mathrm{d},1} \cdot \delta \mathbf{q}_0 + \mathrm{D}_{1+n_{\mathrm{p}}} \tilde{\mathcal{L}}_{\mathrm{d},n_{\mathrm{t}}} \cdot \delta \mathbf{q}_{n_{\mathrm{t}}} \end{aligned} \tag{32}$$

By definition, $\delta\mathbf{q}_0 = \delta\mathbf{q}_{n_\mathrm{t}} = \mathbf{0}$ are always zero. We also define the derivative $\mathrm{D}_{1+i}\tilde{\mathcal{L}}_{\mathrm{d},k+1}$ in the following way:

$$\mathrm{D}_{1+i}\tilde{\mathcal{L}}_{\mathrm{d},k+1} = \frac{\partial\tilde{\mathcal{L}}_{\mathrm{d},k+1}}{\partial\mathbf{q}_{k+\frac{i}{n_\mathrm{p}}}} \quad \text{with} \quad i \in \{0,\dots n_\mathrm{p}\} \tag{33}$$

We collect the terms for similar variations and get:

$$\mathbf{0} = \mathrm{D}_{1+n_\mathrm{p}}\tilde{\mathcal{L}}_{\mathrm{d},k} + \mathrm{D}_1\tilde{\mathcal{L}}_{\mathrm{d},k+1} \tag{34}$$

$$\mathbf{0} = \mathrm{D}_{1+i}\tilde{\mathcal{L}}_{\mathrm{d},k+1} \quad \forall\, i = 1,\dots,n_\mathrm{p}-1 \tag{35}$$

In the same way, we define the vector of linear momentum. The vector of linear momentum only exists at every macro time step.

$$\bar{\mathbf{p}}^{\mathrm{tot}} = \left[\mathbf{p}_0, \mathbf{p}_1, \mathbf{p}_2, \dots, \mathbf{p}_{n_\mathrm{t}-1}, \mathbf{p}_{n_\mathrm{t}}\right]^{\mathrm{T}} \tag{36}$$

The discrete EULER-LAGRANGE equations are invariant up to rigid body motions. Therefore, we can reformulate the EULER-LAGRANGE equations in the so called position-momentum form [7].

$$\mathbf{p}_k = \mathrm{D}_{1+n_\mathrm{p}}\tilde{\mathcal{L}}_{\mathrm{d},k} = -\mathrm{D}_1\tilde{\mathcal{L}}_{\mathrm{d},k+1} \tag{37}$$

$$-\mathbf{p}_k = \mathrm{D}_1\tilde{\mathcal{L}}_{\mathrm{d},k+1} \tag{38}$$

$$\mathbf{p}_{k+1} = \mathrm{D}_{1+n_\mathrm{p}}\tilde{\mathcal{L}}_{\mathrm{d},k+1} \tag{39}$$

The variation with respect to $\bar{\boldsymbol{\lambda}}^{\mathrm{tot}}$ gives:

$$\frac{\partial}{\partial\bar{\boldsymbol{\lambda}}^{\mathrm{tot}}}\left(\sum_{k=0}^{n_\mathrm{t}-1}\tilde{\mathcal{L}}_{\mathrm{d},k+1}\right)\cdot\delta\bar{\boldsymbol{\lambda}}^{\mathrm{tot}} = -\sum_{k=0}^{n_\mathrm{t}-1}h_n\sum_{i=0}^{n_\mathrm{p}}\boldsymbol{\Phi}\left(\mathbf{q}_{k+\frac{i}{n_\mathrm{p}}}\right)\cdot\delta\bar{\boldsymbol{\lambda}}_{k+\frac{i}{n_\mathrm{p}}} \tag{40}$$

As a result, the constraints have to be fulfilled at every micro time step.

$$\boldsymbol{\Phi}\left(\mathbf{q}_{k+\frac{i}{n_\mathrm{p}}}\right)\Big|_{i=0}^{n_\mathrm{p}-1} = \mathbf{0} \tag{41}$$

In order to guarantee the symplecticity construction for our time step scheme, the following condition has to be implemented to fulfill the constraints on velocity level at the last micro time step in every macro time step [2], [7].

$$\frac{\mathrm{d}\boldsymbol{\Phi}\left(\mathbf{q}_{k+1}\right)}{\mathrm{d}t} = \boldsymbol{\Psi}\left(\mathbf{q}_{k+1},\mathbf{p}_{k+1}\right) = \mathbf{0} \tag{42}$$

With the equations below we get the discrete EULER-LAGRANGE equations in the position-momentum form. In these equations we first calculate implicitly the unknown values of the postion vector for every micro time step and the unknown LAGRANGE multiplier in Equation (43). In the "update" step we calculate also implicitly the unknown LAGRANGE multiplier

and the linear momentum vector at the end of the micro time step, Equation (44) [6], [9].

$$
\begin{aligned}
-\mathbf{p}_k &= \frac{\partial \mathcal{L}_{\mathrm{d},k+1}}{\partial \mathbf{q}_k} - h_n \left(\frac{\partial \mathbf{\Phi}(\mathbf{q}_k)}{\partial \mathbf{q}_k} \right)^{\mathrm{T}} \cdot \boldsymbol{\lambda}_k \qquad (43)\\
\mathbf{0} &= \frac{\partial \mathcal{L}_{\mathrm{d},k+1}}{\partial \mathbf{q}_{k+\frac{i}{n_\mathrm{p}}}} - h_n \left(\frac{\partial \mathbf{\Phi}\left(\mathbf{q}_{k+\frac{i}{n_\mathrm{p}}}\right)}{\partial \mathbf{q}_{k+\frac{i}{n_\mathrm{p}}}} \right)^{\mathrm{T}} \cdot \boldsymbol{\lambda}_{k+\frac{i}{n_\mathrm{p}}} \Bigg|_{i=1}^{n_\mathrm{p}-1}\\
\mathbf{0} &= \mathbf{\Phi}(\mathbf{q}_{k+\frac{i}{n_\mathrm{p}}}) \Big|_{i=1}^{n_\mathrm{p}-1}\\
\mathbf{p}_{k+1} &= \frac{\partial \mathcal{L}_{\mathrm{d},k+1}}{\partial \mathbf{q}_{k+1}} - h_n \left(\frac{\partial \mathbf{\Phi}(\mathbf{q}_{k+1})}{\partial \mathbf{q}_{k+1}} \right)^{\mathrm{T}} \cdot \boldsymbol{\lambda}_{k+1} \qquad (44)\\
\mathbf{0} &= \mathbf{\Psi}\left(\mathbf{q}_{k+1}, \mathbf{p}_{k+1}\right)
\end{aligned}
$$

The derivative of the discrete LAGRANGE function with respect to $\mathbf{q}$ for every element can be written as

$$
\begin{aligned}
\frac{\partial \mathcal{L}_{\mathrm{d},k+1}}{\partial \bar{\mathbf{q}}^e_{k+1}} &= \sum_{i=1}^{n_\mathrm{q}} w_i \frac{\partial \left(\frac{1}{2} \mathbf{q}^{\mathrm{d}^e}(\alpha_i) \cdot \mathbb{M}^e \cdot \mathbf{q}^{\mathrm{d}^e}(\alpha_i) \right)}{\partial \bar{\mathbf{q}}^e_{k+1}} \qquad (45)\\
&- \sum_{i=1}^{n_\mathrm{q}} w_i \frac{\partial \left(\int\limits_{\mathcal{B}_0^e} \left[\rho_0 \psi^e \left(\tilde{\mathbf{C}}^e(\mathbf{q}^{\mathrm{h}^e}(\alpha_i)) \right) + \rho_0 \mathbf{g}^e \cdot \mathbf{q}^{\mathrm{h}^e} \right] \mathrm{d}V \right)}{\partial \bar{\mathbf{q}}^e_{k+1}}.
\end{aligned}
$$

4 CONSERVATION PROPERTIES

Every variational integrator conserves the balance of total linear momentum and the balance of total angular momentum. Without any constrains and no gravitational force, it is easy to calculate these conservation properties, but we want to show how these properties can be calculated and show that they are preserved, and hence constraints and a gravity force are included in the simulation.

4.1 BALANCE OF TOTAL LINEAR MOMENTUM

In the case without a DIRICHLET boundary, the conservation of the balance of total linear momentum in the x, y, z-direction can be calculated by the sum over all n_nodes nodes:

$$
\underbrace{\sum_{i=1}^{n_\mathrm{nodes}} \left[\mathbf{p}_{j,i_{k+1}} - \mathbf{p}_{j,i_k} \right]}_{P_{i+1} - P_i} = 0 \qquad \forall j = [x, y, z] \qquad (46)
$$

In the case with boundary nodes, the conservation of the balance of total linear momentum in the x, y, z-direction can be calculated by the sum over all n_nodes nodes and the sum over the

LAGRANGE multiplier vector:

$$\sum_{i=1}^{n_{\text{nodes}}} \left[\mathbf{p}_{j,i_{k+1}} - \mathbf{p}_{j,i_k}\right] + h_n \sum_{i=1}^{n_{\text{nodes}}} \sum_{m=0}^{n_{\text{p}}} \boldsymbol{\lambda}_{j,i_{k+\frac{m}{n_{\text{p}}}}} = 0 \qquad \forall j = [x,y,z] \quad (47)$$

$$\underbrace{\sum_{i=1}^{n_{\text{nodes}}} \left[\mathbf{p}_{j,i_{k+1}} - \mathbf{p}_{j,i_k}\right]}_{P_{i+1}-P_i} + \underbrace{h_n \sum_{i=1}^{n_{\text{nodes}}} \sum_{m=0}^{n_{\text{p}}} w_{\text{c}} M_{\text{c},m}(\alpha_{\text{c}}) \tilde{\boldsymbol{\lambda}}_{j,i_{k+\frac{m}{n_{\text{p}}}}}}_{\bar{F}^{\text{ext}}} = 0 \qquad \forall j = [x,y,z] \quad (48)$$

4.2 BALANCE OF TOTAL ANGULAR MOMENTUM

Without a DIRICHLET boundary and external forces, the conservation of the balance of total angular momentum can be easily calculated by

$$\underbrace{\sum_{i=1}^{n_{\text{nodes}}} \left[\mathbf{q}_{i_{k+1}} \times \mathbf{p}_{i_{k+1}} - \mathbf{q}_{i_k} \times \mathbf{p}_{i_k}\right]}_{L_{i+1}-L_i} = \mathbf{0} \quad (49)$$

In the case of DIRICHLET boundary conditions, the bearing forces at the boundary nodes have to be calculated. Also the gravity force has to be included in the calculation to show the conservation of the balance of the balance of total angular momentum.

$$\underbrace{\sum_{i=1}^{n_{\text{nodes}}} \left[\mathbf{q}_{i_{k+1}} \times \mathbf{p}_{i_{k+1}} - \mathbf{q}_{i_k} \times \mathbf{p}_{i_k}\right]}_{L_{i+1}-L_i} + \underbrace{\sum_{i=1}^{n_{\text{nodes}}} \left[\sum_{m=0}^{n_{\text{p}}} M_m(\alpha) \mathbf{q}_{i,m_{k+\frac{m}{n_{\text{p}}}}} \times \mathbf{F}^{\text{ext},h}_{i_{k+\frac{m}{n_{\text{p}}}}}\right]}_{\bar{M}^{\text{ext}}} = \mathbf{0} \quad (50)$$

Then the approximated external forces $\mathbf{F}^{\text{ext},h}_{i_{k+\frac{m}{n_{\text{p}}}}}$ only depends on the gravitational force $\mathbf{F}_{\text{g}}$, and the external forces are equal to the gravity force.

$$\mathbf{F}^{\text{ext},h}_{i_{k+\frac{m}{n_{\text{p}}}}} = \mathbf{F}_{\text{g}} \quad (51)$$

In the case with boundary nodes the bearing forces at the boundary nodes have to be calculated. Therefore, we introduce a force $\mathbf{F}_\lambda$ which is theoretically approximated at the GAUSSIAN points in time and the force $\mathbf{F}_{\lambda\text{c}}$. Now we project $\mathbf{F}_{\lambda\text{c}}$ onto $\mathbf{F}_\lambda$ with the following relation.

$$\bar{\mathbf{M}}_{\text{g}} \mathbf{w}_{\text{g}} \mathbf{M}_{\text{g}} \mathbf{F}_\lambda = \bar{\mathbf{M}}_{\text{c}} \mathbf{w}_{\text{c}} \mathbf{M}_{\text{c}} \mathbf{F}_{\lambda\text{c}} \quad (52)$$

$$\bar{\mathbf{M}}_{\text{g}} \mathbf{w}_{\text{g}} \left(\mathbf{M}^{\text{n}}_{\text{g}} \mathbf{F}^{\text{n}}_\lambda + \mathbf{M}^{1}_{\text{g}} \mathbf{F}^{1}_\lambda\right) = \bar{\mathbf{M}}_{\text{c}} \mathbf{w}_{\text{c}} \mathbf{M}_{\text{c}} \mathbf{F}_{\lambda\text{c}} \quad (53)$$

$$\bar{\mathbf{M}}_{\text{g}} \mathbf{w}_{\text{g}} \mathbf{M}^{\text{n}}_{\text{g}} \mathbf{F}^{\text{n}}_\lambda = \bar{\mathbf{M}}_{\text{c}} \mathbf{w}_{\text{c}} \mathbf{M}_{\text{c}} \mathbf{F}_{\lambda\text{c}} - \bar{\mathbf{M}}_{\text{g}} \mathbf{w}_{\text{g}} \mathbf{M}^{1}_{\text{g}} \mathbf{F}^{1}_\lambda \quad (54)$$

$$\mathbf{F}^{\text{n}}_\lambda = \left(\bar{\mathbf{M}}_{\text{g}} \mathbf{w}_{\text{g}} \mathbf{M}^{\text{n}}_{\text{g}}\right)^{-1} \left[\bar{\mathbf{M}}_{\text{c}} \underbrace{\mathbf{w}_{\text{c}} \mathbf{M}_{\text{c}} \mathbf{F}_{\lambda\text{c}}}_{\tilde{\boldsymbol{\lambda}}_{\text{F}}} - \bar{\mathbf{M}}_{\text{g}} \mathbf{w}_{\text{g}} \mathbf{M}^{1}_{\text{g}} \mathbf{F}^{1}_\lambda\right] \quad (55)$$

$$\mathbf{F}^{\text{n}}_\lambda = \left(\bar{\mathbf{M}}_{\text{g}} \mathbf{w}_{\text{g}} \mathbf{M}^{\text{n}}_{\text{g}}\right)^{-1} \left[\bar{\mathbf{M}}_{\text{c}} \tilde{\boldsymbol{\lambda}}_{\text{F}} - \bar{\mathbf{M}}_{\text{g}} \mathbf{w}_{\text{g}} \mathbf{M}^{1}_{\text{g}} \mathbf{F}^{1}_\lambda\right] \quad (56)$$

$\bar{\mathbf{M}}_{\text{g}}$ and $\bar{\mathbf{M}}_{\text{c}}$ are trial functions for a GAUSSIAN and NEWTON-COTÊS quadrature. $\mathbf{M}_{\text{g}}$ and $\mathbf{M}_{\text{c}}$ are also shape functions for a GAUSSIAN and NEWTON-COTÊS quadrature at all quadrature

points and the corresponding quadrature weights $\mathbf{w}_\mathrm{g}$ and $\mathbf{w}_\mathrm{c}$. $\mathbf{F}_\lambda^\mathrm{n}$ represents the unknown vector of the forces in one macro time step.
Furthermore, a non-diagonal mass matrix is used and presented in the time step scheme, because it is essential to calculate the terms from nondiagonal entries in the mass matrix multiplied with the approximated velocity. We subtract the linear momentum values $\mathbf{p}_\mathrm{kin}^\mathrm{bc}$ from the calculated LAGRANGE multiplier vector $\boldsymbol{\lambda}$.

$$h_n\tilde{\boldsymbol{\lambda}}_\mathrm{F} = h_n\boldsymbol{\lambda} - \mathbf{p}_\mathrm{kin}^\mathrm{bc} \tag{57}$$

$$\tilde{\boldsymbol{\lambda}}_\mathrm{F} = \boldsymbol{\lambda} - \frac{\mathbf{p}_\mathrm{kin}^\mathrm{bc}}{h_n} \tag{58}$$

$$\mathbf{p}_\mathrm{kin}^\mathrm{nd} = \mathbb{M}\cdot\dot{\mathbf{q}} = \sum_{i=1}^{n_\mathrm{q}} M'(\alpha_i)w_i\frac{[\mathbb{M}-\mathrm{diag}(\mathbb{M})]\cdot\mathbf{q}^\mathrm{d}(\alpha_i)}{h_n} \tag{59}$$

For the calculation of the force vector $\tilde{\boldsymbol{\lambda}}_\mathrm{F}$ only the values at boundary nodes $\mathbf{p}_\mathrm{kin}^\mathrm{bc}$ are needed.

$$\mathbf{p}_\mathrm{kin}^\mathrm{bc} = \left.\mathbf{p}_\mathrm{kin}^\mathrm{nd}\right|_\mathrm{boundary} \tag{60}$$

$$\tilde{\boldsymbol{\lambda}}_\mathrm{F} = \boldsymbol{\lambda} - \frac{\mathbf{p}_\mathrm{kin}^\mathrm{bc}}{h_n} = \boldsymbol{\lambda} - \mathbf{F}_\mathrm{kin}^\mathrm{bc} \tag{61}$$

Now we use Equation (56) and calculate for every macro time step the unknown forces at the nodes $\mathbf{F}_\lambda^\mathrm{n}$ for every micro time step.
The calculated forces can now be used for the calculation of balance of the total angular momentum in Equation (50). We now define $\mathbf{F}^{\mathrm{ext},h}_{i_{k+\frac{m}{n_\mathrm{p}}}}$ as

$$\mathbf{F}^{\mathrm{ext},h}_{i_{k+\frac{m}{n_\mathrm{p}}}} = \mathbf{F}_\mathrm{g} + \sum_{m=0}^{n_\mathrm{p}} wM_m(\alpha)\mathbf{F}_{\lambda,i_{k+\frac{m}{n_\mathrm{p}}}} \tag{62}$$

Hence, it is possible to show the conservation of the balance of total angular momentum in the x, y, z-direction for a system with homolonic constraints.

4.3 THE DISCRETE GRADIENT

We start analogous to [1] with two functionals $\mathcal{F}^e$ and $\mathcal{G}^e$.

$$\mathcal{F}^e(\mathbf{D}^\mathrm{G}W_e(\alpha)) = \frac{1}{2}\int_0^1 \left\|\mathbf{D}^\mathrm{G}W_e(\alpha) - \mathbf{D}W_e(\alpha)\right\|^2 \mathrm{d}\alpha \tag{63}$$

$$\mathcal{G}^e(\mathbf{D}^\mathrm{G}W_e(\alpha)) = W_e(1) - W_e(0) - \int_0^1 \mathbf{D}^\mathrm{G}W_e(\alpha) : \frac{\partial\mathbf{C}}{\partial\alpha}\mathrm{d}\alpha \tag{64}$$

We choose the functional $\mathcal{G}^e$ as a constraint for every element with a LAGRANGE multiplier γ_e. The new functional $\mathcal{H}^e$ should only depend on $\mathbf{D}^\mathrm{G}W_e(\alpha)$ and γ_e

$$\mathcal{H}^e(\mathbf{D}^\mathrm{G}W_e(\alpha), \gamma_e) = \mathcal{F}^e(\mathbf{D}^\mathrm{G}W_e(\alpha)) + \gamma_e\mathcal{G}^e(\mathbf{D}^\mathrm{G}W_e(\alpha)) \tag{65}$$

The variation of $\mathcal{H}^e$ with respect to $\mathbf{D}^{\mathrm{G}}W_e(\alpha)$ gives us the first equation

$$\frac{\partial \mathcal{H}^e}{\partial \mathbf{D}^{\mathrm{G}}W_e(\alpha)} = \int_0^1 \left[\left(\mathbf{D}^{\mathrm{G}}W_e(\alpha) - \mathbf{D}W_e(\alpha) \right) - \gamma_e \frac{\partial \mathbf{C}(\alpha)}{\partial \alpha} \right] \mathrm{d}\alpha \delta \mathbf{D}^{\mathrm{G}}W_e(\alpha) = \mathbf{0} \quad (66)$$

$$\mathbf{0} = \left(\mathbf{D}^{\mathrm{G}}W_e(\alpha) - \mathbf{D}W_e(\alpha) \right) - \gamma_e \frac{\partial \mathbf{C}(\alpha)}{\partial \alpha} \quad (67)$$

$$\mathbf{D}^{\mathrm{G}}W_e(\alpha) = \mathbf{D}W_e(\alpha) + \gamma_e \frac{\partial \mathbf{C}(\alpha)}{\partial \alpha} \quad (68)$$

The variation of $\mathcal{H}^e$ with respect to γ_e gives us the second equation

$$\frac{\partial \mathcal{H}^e}{\partial \gamma_e} = \left[W_e(1) - W_e(0) - \int_0^1 \mathbf{D}^{\mathrm{G}}W_e(\alpha) : \frac{\partial \mathbf{C}(\alpha)}{\partial \alpha} \mathrm{d}\alpha \right] \delta \gamma_e = \mathbf{0} \quad (69)$$

$$0 = W_e(1) - W_e(0) - \int_0^1 \mathbf{D}^{\mathrm{G}}W_e(\alpha) : \frac{\partial \mathbf{C}(\alpha)}{\partial \alpha} \mathrm{d}\alpha \quad (70)$$

Now we replace the $\mathbf{D}^{\mathrm{G}}W_e(\alpha)$ term in the Equation (70) with $\mathbf{D}^{\mathrm{G}}W_e(\alpha)$ from Equation (68).

$$\mathbf{D}^{\mathrm{G}}W_e(\alpha) = \mathbf{D}W_e(\alpha) + \gamma_e \frac{\partial \mathbf{C}(\alpha)}{\partial \alpha} \quad (71)$$

$$W_e(1) - W_e(0) = \int_0^1 \mathbf{D}W_e(\alpha) : \frac{\partial \mathbf{C}(\alpha)}{\partial \alpha} \mathrm{d}\alpha + \gamma_e \int_0^1 \frac{\partial \mathbf{C}(\alpha)}{\partial \alpha} : \frac{\partial \mathbf{C}(\alpha)}{\partial \alpha} \mathrm{d}\alpha \quad (72)$$

Rearranging the equation with respect to γ_e and replacing it in Equation (68) we obtain

$$\gamma_e = \frac{W_e(1) - W_e(0) - \int_0^1 \mathbf{D}W_e(\alpha) : \frac{\partial \mathbf{C}(\alpha)}{\partial \alpha} \mathrm{d}\alpha}{\int_0^1 \frac{\partial \mathbf{C}(\alpha)}{\partial \alpha} : \frac{\partial \mathbf{C}(\alpha)}{\partial \alpha} \mathrm{d}\alpha} \quad (73)$$

$$\mathbf{D}^{\mathrm{G}}W_e(\alpha) = \mathbf{D}W_e(\alpha) + \frac{W_e(1) - W_e(0) - \int_0^1 \mathbf{D}W_e(\alpha) : \frac{\partial \mathbf{C}(\alpha)}{\partial \alpha} \mathrm{d}\alpha}{\int_0^1 \frac{\partial \mathbf{C}(\alpha)}{\partial \alpha} : \frac{\partial \mathbf{C}(\alpha)}{\partial \alpha} \mathrm{d}\alpha} \frac{\partial \mathbf{C}(\alpha)}{\partial \alpha} \quad (74)$$

Until now, the approximation of $\mathbf{C}(\alpha)$ and $\mathbf{D}W_e(\alpha)$ are not fixed. So we take a look at which kind of possiblities we have to choose an approximation. To fulfill the balance of energy in every time step, we define integral over one time step as

$$\int_0^1 \frac{\mathrm{d}W_e(\alpha)}{\mathrm{d}\alpha} \mathrm{d}\alpha = \int_0^1 \tilde{\mathbf{S}}(\alpha) : \frac{1}{2} \frac{\partial \mathbf{C}(\alpha)}{\partial \alpha} \mathrm{d}\alpha = \int_0^1 \tilde{\mathbf{S}}(\alpha) : \frac{1}{2} \frac{\partial \mathbf{C}(\alpha)}{\partial \mathbf{q}^{\mathrm{h}}} \frac{\partial \mathbf{q}^{\mathrm{h}}}{\partial \alpha} \mathrm{d}\alpha = W_e(1) - W_e(0). \quad (75)$$

To fulfill Equation (75), a special $\tilde{\mathbf{S}}(\alpha)$ is needed. We define $\tilde{\mathbf{S}}(\alpha) \equiv 2\mathbf{D}^{\mathrm{G}}W_e(\alpha)$ and test the relation.

$$\begin{aligned} W_e(1) - W_e(0) &= \int_0^1 \tilde{\mathbf{S}}(\alpha) : \frac{1}{2}\frac{\partial \mathbf{C}(\alpha)}{\partial \alpha} \mathrm{d}\alpha \\ &= \int_0^1 \mathbf{D}W_e(\alpha) : \frac{\partial \mathbf{C}(\alpha)}{\partial \alpha} \mathrm{d}\alpha \\ &+ \frac{W_e(1) - W_e(0) - \int_0^1 \mathbf{D}W_e(\alpha) : \frac{\partial \mathbf{C}(\alpha)}{\partial \alpha} \mathrm{d}\alpha}{\int_0^1 \frac{\partial \mathbf{C}(\alpha)}{\partial \alpha} : \frac{\partial \mathbf{C}(\alpha)}{\partial \alpha} \mathrm{d}\alpha} \int_0^1 \frac{\partial \mathbf{C}(\alpha)}{\partial \alpha} : \frac{\partial \mathbf{C}(\alpha)}{\partial \alpha} \mathrm{d}\alpha \\ W_e(1) - W_e(0) &= W_e(1) - W_e(0) \end{aligned} \tag{76}$$

It is possible to choose a different approximation of $\mathbf{C}$ and also fulfill Equation (75).

$$\int_0^1 \mathbf{D}W_e(\alpha) : \frac{\partial \mathbf{C}_a}{\partial \alpha} \mathrm{d}\alpha + \frac{W_e(1) - W_e(0) - \int_0^1 \mathbf{D}W_e(\alpha) : \frac{\partial \mathbf{C}_a}{\partial \alpha} \mathrm{d}\alpha}{\int_0^1 \frac{\partial \mathbf{C}_b}{\partial \alpha} : \frac{\partial \mathbf{C}_a}{\partial \alpha} \mathrm{d}\alpha} \int_0^1 \frac{\partial \mathbf{C}_b}{\partial \alpha} : \frac{\partial \mathbf{C}_a}{\partial \alpha} \mathrm{d}\alpha \tag{77}$$

One possible case is:

$$\begin{aligned} \mathbf{C}_a &\equiv \mathbf{C}(\mathbf{q}^{\mathrm{h}}) \\ \mathbf{C}_b = \mathbf{C}_a \quad &\text{and} \quad \mathbf{D}W_e(\alpha) = \mathbf{D}W_e(\mathbf{C}_a) \end{aligned} \tag{78}$$

One other case is:

$$\begin{aligned} \mathbf{C}_a &\equiv \mathbf{C}(\mathbf{q}^{\mathrm{h}}) \\ \mathbf{C}_b = \mathbf{C}^{\mathrm{h}} \neq \mathbf{C}_a \quad &\text{and} \quad \mathbf{D}W_e(\alpha) = \mathbf{D}W_e(\mathbf{C}_b) \end{aligned} \tag{79}$$

This special choice of $\mathbf{C}_a$ and $\mathbf{C}_b$ is also known as assumed strain formulation [1].

4.4 ENERGY CONSERVING

A variational integrator only bind the energy error in every time step, but not under the NEWTON tolerance. We implement a discrete gradient to correct energy error [8], [1]. The variational integrator loses its symplecticity, but the absolute value of the energy error in every time step is bounded by the NEWTON tolerance. Splitting Equation (74) in two parts allows us to put one part in potential energy and the other part can be introduced by the LAGRANGE-

D'ALEMBERT principle.

$$\begin{aligned}\int\limits_{\mathcal{B}_0^e} \frac{\partial \rho_0 \psi^e\left(\mathbf{C}^{\mathrm{h}^e}\right)}{\partial \bar{\mathbf{q}}_{k+1}^e} \mathrm{d}V &= \int\limits_{\mathcal{B}_0^e} \mathbf{S}^e\left(\mathbf{C}^{\mathrm{h}^e}\right) : \mathbb{B}^e\left(\mathbf{q}^{\mathrm{h}^e}(\alpha)\right) \mathrm{d}V \\ &= \int\limits_{\mathcal{B}_0^e} 2\mathbf{D}W_e(\mathbf{C}^{\mathrm{h}^e}) : \mathbb{B}^e\left(\mathbf{q}^{\mathrm{h}^e}(\alpha)\right) \mathrm{d}V\end{aligned} \tag{80}$$

The second part will be placed in the LAGRANGE-D'ALEMBERT principle.

$$\mathcal{K}^{DG}\left(\mathbf{C}(\alpha)\right) = 2 \frac{W_e(1) - W_e(0) - \int\limits_0^1 \mathbf{D}W_e(\alpha) : \frac{\partial \mathbf{C}(\alpha)}{\partial \alpha} \mathrm{d}\alpha}{\int\limits_0^1 \frac{\partial \mathbf{C}(\alpha)}{\partial \alpha} : \frac{\partial \mathbf{C}(\alpha)}{\partial \alpha} \mathrm{d}\alpha} \frac{\partial \mathbf{C}(\alpha)}{\partial \alpha} \tag{81}$$

The virtual work can be written as

$$\begin{aligned}\delta W_{\mathrm{d},k+1}(\bar{\mathbf{q}}_{k+1}^e) &= -h_n \sum_{i=1}^{n_\mathrm{q}} w_i \mathcal{K}^{DG}(\mathbf{C}^{\mathrm{h}^e}) : \mathbb{B}^e\left(\mathbf{q}^{\mathrm{h}^e}(\alpha_i)\right) \delta \mathbf{q}^{\mathrm{h}^e}(\alpha_i) \\ &= -\sum_{i=0}^{n_\mathrm{q}} \mathbf{\Gamma}_{k+\frac{i}{n_\mathrm{p}}}^{DG}\left(\mathbf{C}^{\mathrm{h}^e}, \mathbf{q}^{\mathrm{h}^e}\right) \delta \mathbf{q}_{k+\frac{i}{n_\mathrm{p}}}^e\end{aligned} \tag{82}$$

The new time step scheme leads to

$$-\mathbf{p}_k = \frac{\partial \mathcal{L}_{\mathrm{d},k+1}}{\partial \mathbf{q}_k} - h_n \left(\frac{\partial \mathbf{\Phi}(\mathbf{q}_k)}{\partial \mathbf{q}_k}\right)^{\mathrm{T}} \cdot \boldsymbol{\lambda}_k + \mathbf{\Gamma}_k^{DG}\left(\mathbf{C}^{\mathrm{h}^e}, \mathbf{q}^{\mathrm{h}^e}\right) \tag{83}$$

$$\begin{aligned}\mathbf{0} &= \frac{\partial \mathcal{L}_{\mathrm{d},k+1}}{\partial \mathbf{q}_{k+\frac{i}{n_\mathrm{p}}}} - h_n \left(\frac{\partial \mathbf{\Phi}\left(\mathbf{q}_{k+\frac{i}{n_\mathrm{p}}}\right)}{\partial \mathbf{q}_{k+\frac{i}{n_\mathrm{p}}}}\right)^{\mathrm{T}} \cdot \boldsymbol{\lambda}_{k+\frac{i}{n_\mathrm{p}}} + \mathbf{\Gamma}_{k+\frac{i}{n_\mathrm{p}}}^{DG}\left(\mathbf{C}^{\mathrm{h}^e}, \mathbf{q}^{\mathrm{h}^e}\right)\Bigg|_{i=1}^{n_\mathrm{p}-1} \\ \mathbf{0} &= \mathbf{\Phi}(\mathbf{q}_{k+\frac{i}{n_\mathrm{p}}})\Big|_{i=1}^{n_\mathrm{p}}\end{aligned}$$

$$\mathbf{p}_{k+1} = \frac{\partial \mathcal{L}_{\mathrm{d},k+1}}{\partial \mathbf{q}_{k+1}} - h_n \left(\frac{\partial \mathbf{\Phi}(\mathbf{q}_{k+1})}{\partial \mathbf{q}_{k+1}}\right)^{\mathrm{T}} \cdot \boldsymbol{\lambda}_{k+1} + \mathbf{\Gamma}_{k+1}^{DG}\left(\mathbf{C}^{\mathrm{h}^e}, \mathbf{q}^{\mathrm{h}^e}\right) \tag{84}$$

$$\mathbf{0} = \mathbf{\Psi}\left(\mathbf{q}_{k+1}, \mathbf{p}_{k+1}\right)$$

With respect to Equation (77), we define the time step scheme with the following approximation of the right CAUCHY-GREEN tensor as VDG1:

$$\mathbf{C}^{\mathrm{h}^e} \equiv \mathbf{C}^e\left(\mathbf{q}^{\mathrm{h}^e}\right) \quad \text{and} \quad \mathbf{D}W_e\left(\mathbf{C}^{\mathrm{h}^e}\right) = \mathbf{D}W_e\left(\mathbf{C}^e\left(\mathbf{q}^{\mathrm{h}^e}\right)\right) \tag{85}$$

This approximation of the right CAUCHY-GREEN tensor in the time step scheme will be named as VDG2:

$$\mathbf{C}^{\mathrm{h}^e} \equiv \sum_{i=0}^{n_\mathrm{q}} M_i(\alpha) \mathbf{C}_i^e(\mathbf{q}_i) \quad \text{and} \quad \mathbf{D}W_e\left(\mathbf{C}^{\mathrm{h}^e}\right) = \mathbf{D}W_e\left(\mathbf{C}_i^e\right) \tag{86}$$

The difference with respect to the energy error and the stability will be shown for the numerical examples.

5 NUMERICAL EXAMPLES

First we show the convergence for a higher order accuracy in position and linear momentum for a free flying rotor. In the next numerical example we also proof the balance of linear momentum, the balance of angular momentum and the balance of energy for the free flying rotor and the vibration of a cantilever beam.

5.1 CONVERGENCE STUDY FOR THE FREE FLYING HYPERELASTIC ROTOR

The convergence was calculated for a simulation time $t = 1\,\mathrm{s}$. After this time, the values of position and linear momentum vectors were used as $\mathbf{q}_{\mathrm{end}}$ and $\mathbf{p}_{\mathrm{end}}$. The reference solution for $\mathbf{q}_{\mathrm{ref}}$ and $\mathbf{p}_{\mathrm{ref}}$ for every polynomial degree n_{p} was calculated with the smallest time step size $h_n \approx 5 \cdot 10^{-4}$. A convergence study is preformed with the following simulation parameters:

n_{el}	560	n_{dof}	$3156 \cdot n_{\mathrm{p}}$
h_n	$2^{-1,\ldots,-9}\,\mathrm{s}$	T_{end}	$1\,\mathrm{s}$
n_{p}	$1,\ldots,4$	ρ_0	8.93
$\rho_0\lambda$	66.25	$\rho_0\mu$	650
ϵ	$1 \cdot 10^{-8}$	$\mathbf{r}_0$	$[0,0,0.3]^{\mathrm{T}}$
$\boldsymbol{\omega}$	$[1,0,1]^{\mathrm{T}}$	$\mathbf{v}$	$[10,0,15]^{\mathrm{T}}$

Table 1: Simulation parameters for the convergence study

The free flying rotor in the reference configuartion is printed in the Figure 2. The motion is subject to a gravitational force field $\mathbf{g}$, and initiated by an initial translational velocity field $\mathbf{v}$ and an intial angular velocity field $\boldsymbol{\omega}$ with the corresponding position vector $\mathbf{r}_0$.

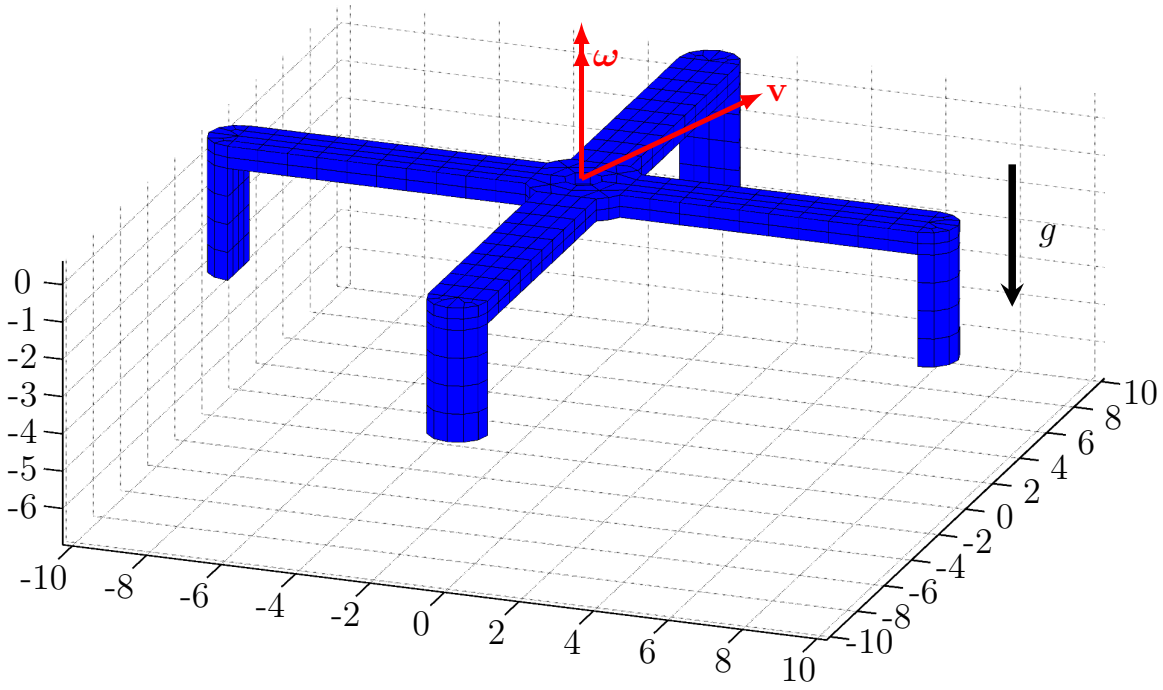

Figure 2: Reference configuration for the free flying hyperelastic rotor for the time $t = 0\,\mathrm{s}$

As error criterion, the relative error in position and linear momentum is defined using the EUCLIDIAN norm. Theoretically, convergence order for position vector and linear momentum vector should be identical; in fact, they are almost identical in dependence of the stiffness of the material. The theoretical values were reached until $n_\mathrm{p} = 3$. For $n_\mathrm{p} = 4$, the theoretical values are not obtained, but we assume that with more calculation points it would be possible to show the theoretical convergence order.

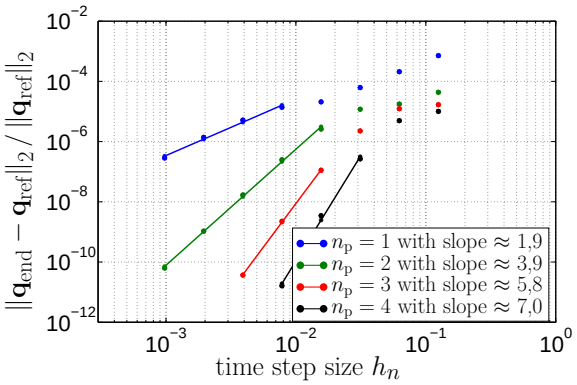

Figure 3: Convergence in position without discrete gradient

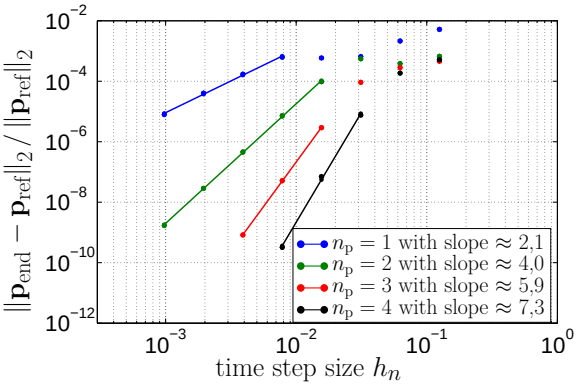

Figure 4: Convergence in linear momentum without discrete gradient

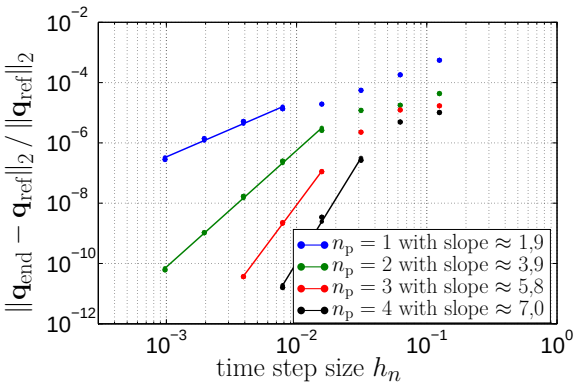

Figure 5: Convergence in position with VDG2

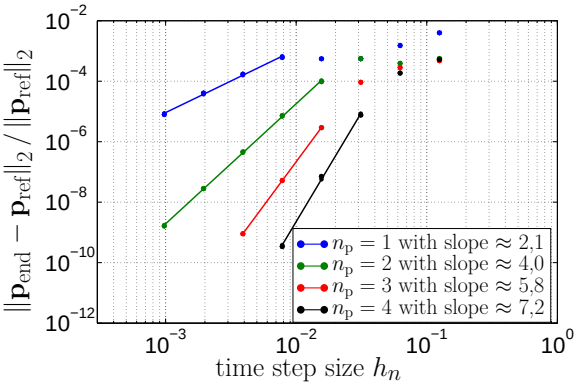

Figure 6: Convergence in linear momentum with VDG2

5.2 FREE FLYING HYPERELASTIC ROTOR

In the Figure 7 the reference configuration of the free flying rotor is shown with a finer mesh. In this example the rotor gets an initial linear velocity $\mathbf{v}$ and an initial angular velocity $\boldsymbol{\omega}$ around the point $\mathbf{r}_0$. The simulation parameters can be found in the Table 2. The printed total CPU-time

n_{el}	18639	n_{dof}	$74136 \cdot n_{\text{p}} = 222408$
h_n	0.02 s	T_{end}	4 s
n_{p}	3	ρ_0	8.93
$\rho_0\lambda$	$66.25 \cdot 10^3$	$\rho_0\mu$	$65 \cdot 10^5$
ϵ	$1 \cdot 10^{-7}$	$\mathbf{r}_0$	$[0, 0, 0.3]^{\text{T}}$
$\boldsymbol{\omega}$	$[1, 0, 1]^{\text{T}}$	$\mathbf{v}$	$[10, 0, 15]^{\text{T}}$
VI without discrete gradient			
t_{cpu}	14790 s	t_{solver}	11660 s
VDG2			
t_{cpu}	17660 s	t_{solver}	12380 s

Table 2: Simulation parameters for the free flying rotor

and SOLVER-time in the table both are measured for a parallelization of the element calculation in CUDA. For a large number of degrees of freedom n_{dof} resulting from the polynomial degree n_{p} for the selected approximation, the CPU-time t_{cpu} more and more depends on the SOLVER-time t_{solver}.
The overhead for a calculation with a higher order approximation and the effort of using a discrete gradient in the element routine can be compensated by a parallelization of the element routine with CUDA.

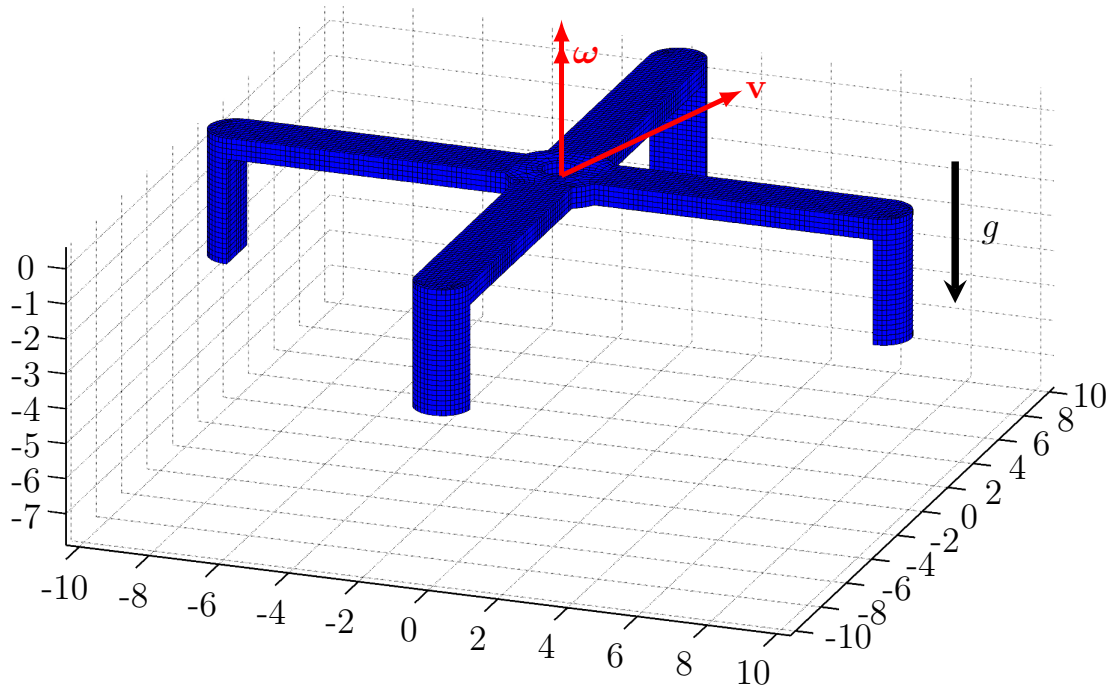

Figure 7: Reference configuration for the free flying hyperelastic rotor for the time $t = 0$ s

The Figures 8-11 show the parabolic free fly of the rotor in the gravitational field for different time points. The color bar at the right-hand side of each figure marks the VON MISES stress at the spatial nodes.

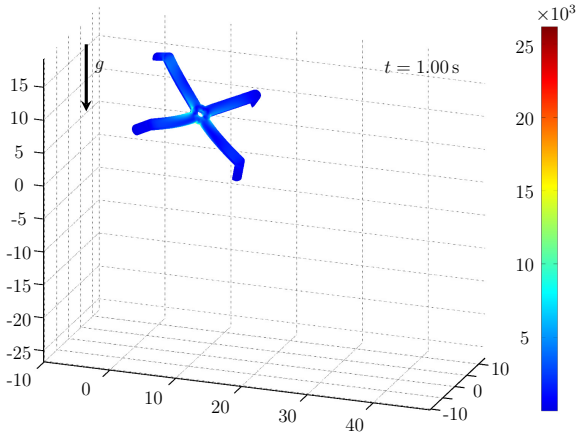

Figure 8: Actual configuration for the free flying hyperelastic rotor for the time $t = 1\,\mathrm{s}$

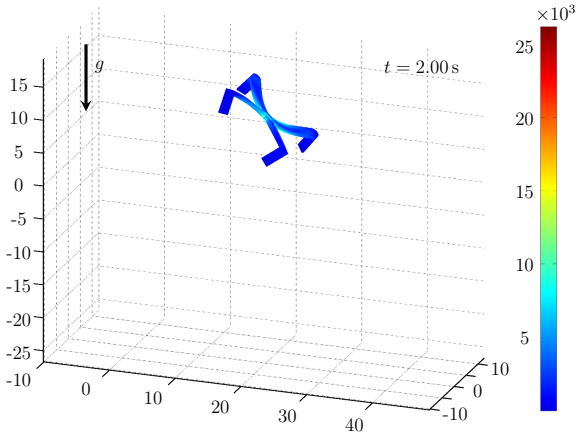

Figure 9: Actual configuration for the free flying hyperelastic rotor for the time $t = 2\,\mathrm{s}$

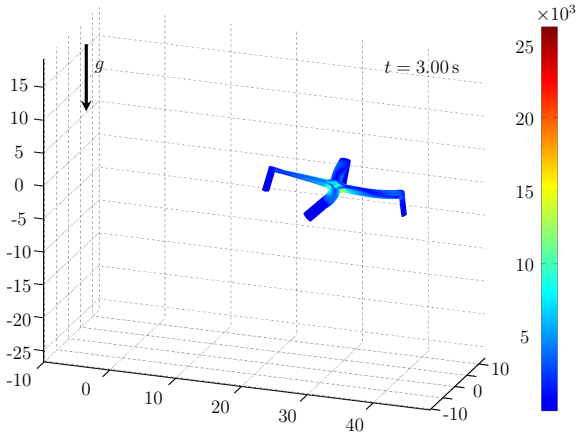

Figure 10: Actual configuration for the free flying hyperelastic rotor for the time $t = 3\,\mathrm{s}$

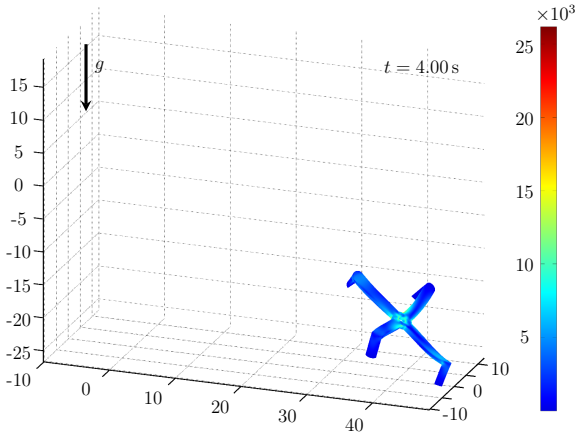

Figure 11: Actual configuration for the free flying hyperelastic rotor for the time $t = 4\,\mathrm{s}$

For this simulation, we calculated the balance of total linear momentum, the balance of total angular momentum, and the balance of total energy for a higher order variational integrator without using a discrete gradient. All balances were also divided by the NEWTON criterion ϵ, see Table 2. The balances of total linear momentum and balance of total angular momentum

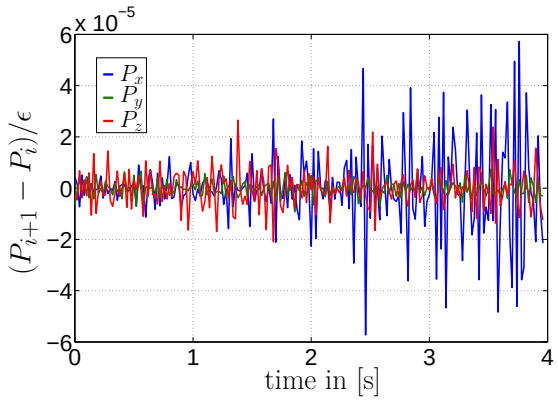

Figure 12: Balance of total linear momentum without discrete gradient for free flying rotor with $n_\mathrm{p} = 2$

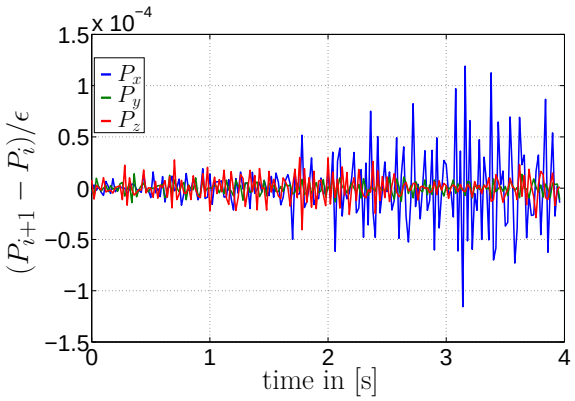

Figure 13: Balance of total linear momentum without discrete gradient for free flying rotor with $n_\mathrm{p} = 3$

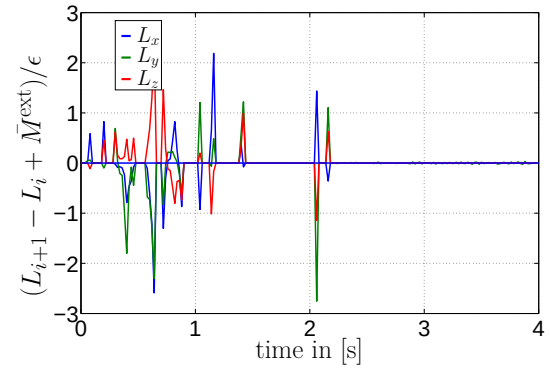

Figure 14: Balance of total angular momentum without discrete gradient for free flying rotor with $n_\mathrm{p} = 2$

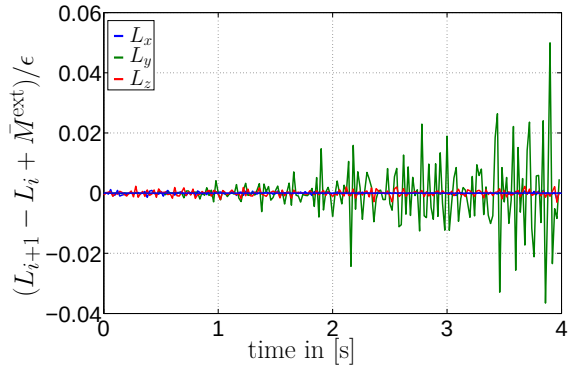

Figure 15: Balance of total angular momentum without discrete gradient for free flying rotor with $n_\mathrm{p} = 3$

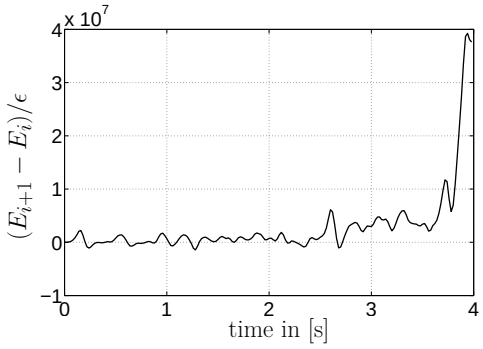

Figure 16: Balance of total energy without discrete gradient for free flying rotor with $n_\mathrm{p} = 2$

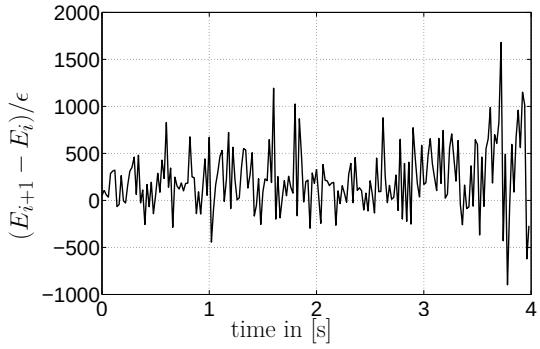

Figure 17: Balance of total energy without discrete gradient for free flying rotor with $n_\mathrm{p} = 3$

are met, but not the balance of total energy. The balance of the total angular momentum is calculated under influence of the gravitational force, see Equation (50).
The same kind of calculations are preformed with the discrete gradient for the time step scheme VDG2. The balance of total linear momentum and balance of total angular momentum are also met.

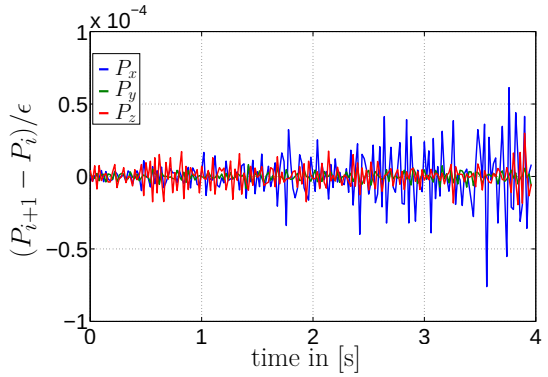

Figure 18: Balance of total linear momentum with VDG2 for free flying rotor with $n_\mathrm{p} = 2$

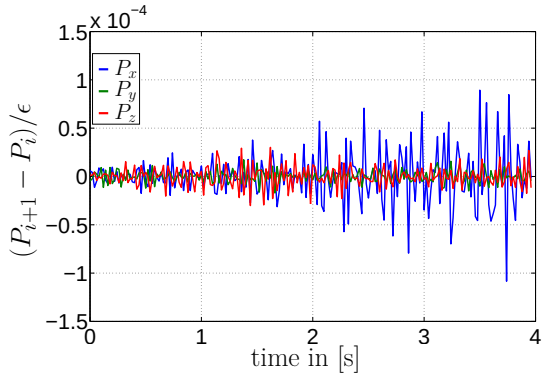

Figure 19: Balance of total linear momentum with VDG2 for free flying rotor with $n_\mathrm{p} = 3$

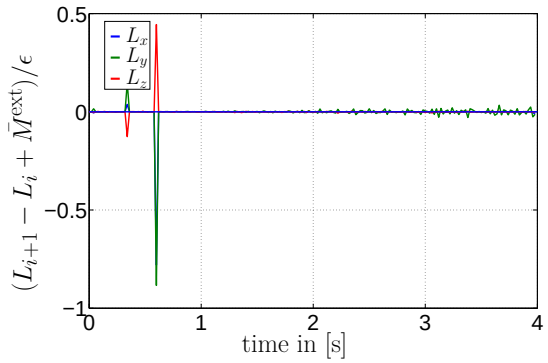

Figure 20: Balance of total angular momentum with VDG2 for free flying rotor with $n_\mathrm{p} = 2$

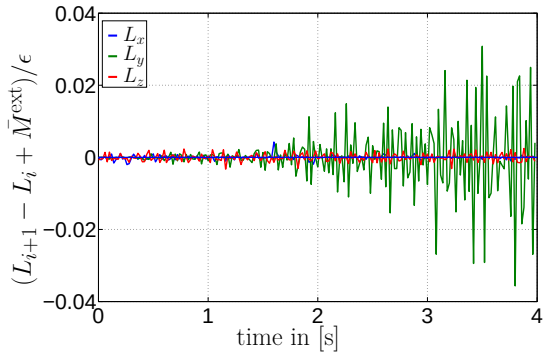

Figure 21: Balance of total angular momentum with VDG2 for free flying rotor with $n_\mathrm{p} = 3$

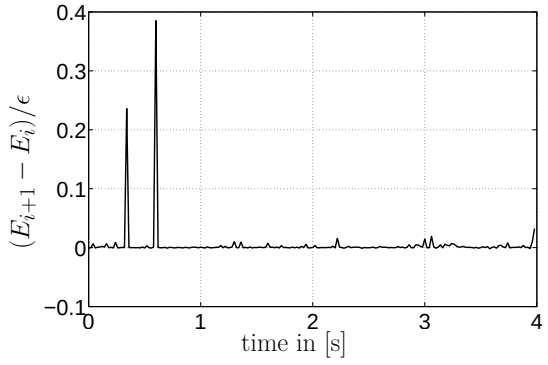

Figure 22: Balance of total energy with VDG2 for free flying rotor with $n_\mathrm{p} = 2$

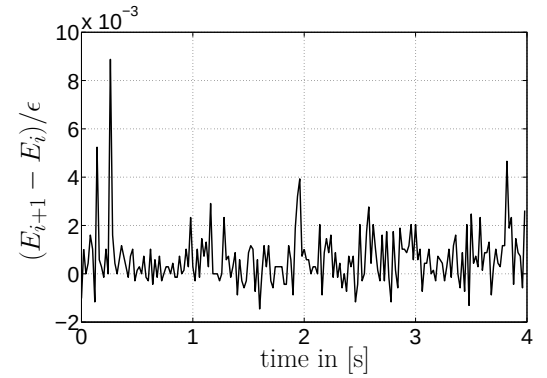

Figure 23: Balance of total energy with VDG2 for free flying rotor with $n_\mathrm{p} = 3$

Importanted are the Figures 22-23 showing the balances of the total energy for VDG2 time step scheme. The absolute value of the error in the balance of total energy for every time step is below the chosen NEWTON criterion ϵ. Hence, the VDG2 time step scheme preserves the total energy over the total simulation time. Another interesting point is the balance of total angular momentum for VDG2 with $n_\mathrm{p} = 2$ Figure 20, here a no peaks over the NEWTON criterion arise. This simulation was calculated with the same parameters like the simulation in Figure 14, but the discrete gradient shows a better fulfillment of the balance of total angular momentum.

5.3 VIBRATION OF HYPERELASTIC CANTILEVER BEAM

The second numerical example is a vibration of a hyperelastic cantilever beam. We used the rotor once more, but now we fixed the degrees of freedom $n_{\text{q,fix}}$ in all directions in the hub of the rotor, see Figure 24. Under influence of the gravitational force, every blade of the rotor starts to swing around the static equilibrium position.

n_{el}	18639	n_{dof}	$74136 \cdot n_{\text{p}} = 222408$
h_n	$0.025\,\text{s}$	T_{end}	$4\,\text{s}$
n_{p}	3	ρ_0	8.93
$\rho_0\lambda$	$16.25 \cdot 10^4$	$\rho_0\mu$	$15 \cdot 10^6$
ϵ	$1 \cdot 10^{-7}$	$n_{\text{q,fix}}$	$360 \cdot n_{\text{p}} = 1080$
VI without discrete gradient			
t_{cpu}	$14560\,\text{s}$	t_{solver}	$11620\,\text{s}$
VDG2			
t_{cpu}	$17850\,\text{s}$	t_{solver}	$12730\,\text{s}$

Table 3: Simulation parameters for the vibration of the hyperelastic cantilever beam

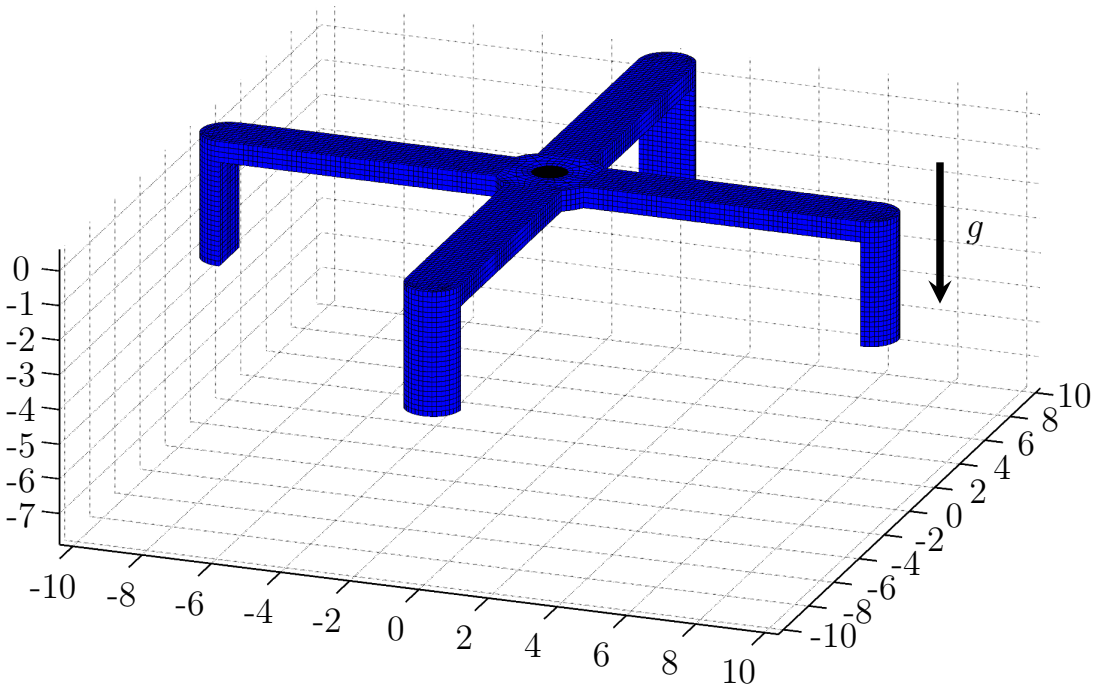

Figure 24: Reference configuration for the hyperelastic cantilever beam for the time $t = 0\,\text{s}$

The Figures 25-30 show the vibration around the static idle position for every blade of the rotor. With the fixed hub, every blade shows the same vibration behavior as the cantilever beam in four directions due to the symmetry. At the time $t = 1.925\,\mathrm{s}$, the blades reach the maximum elongation. After $t = 3.775\,\mathrm{s}$, the vibration of the rotor is again in the initial state.

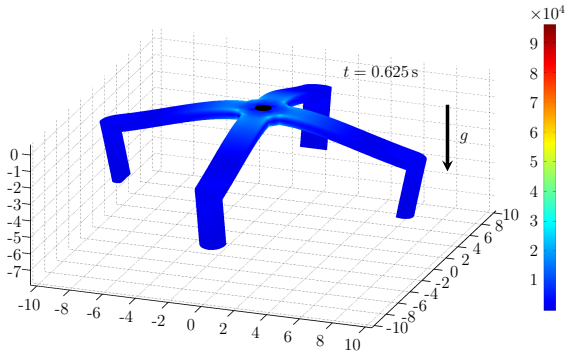

Figure 25: Actual configuration for the hyperelastic cantilever beam for the time $t = 0.625\,\mathrm{s}$

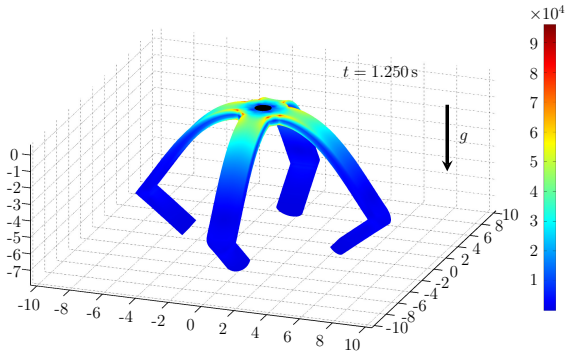

Figure 26: Actual configuration for the hyperelastic cantilever beam for the time $t = 1.25\,\mathrm{s}$

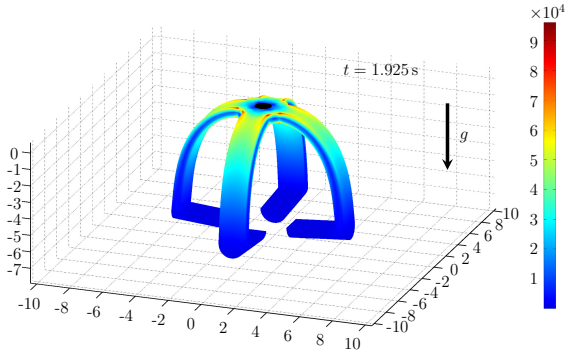

Figure 27: Actual configuration for the hyperelastic cantilever beam for the time $t = 1.925\,\mathrm{s}$

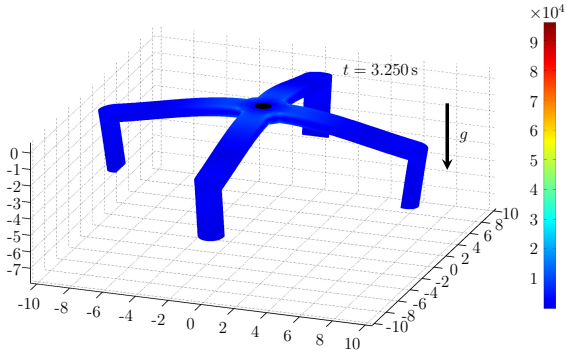

Figure 28: Actual configuration for the hyperelastic cantilever beam for the time $t = 3.25\,\mathrm{s}$

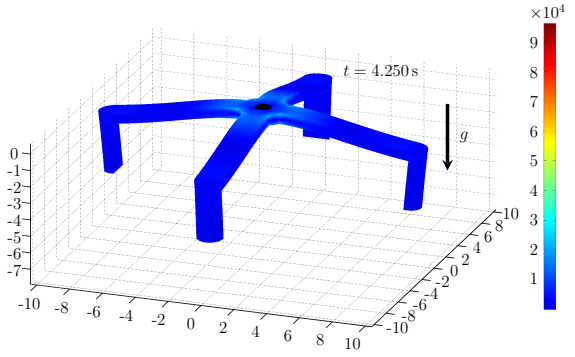

Figure 29: Actual configuration for the hyperelastic cantilever beam for the time $t = 4.25\,\mathrm{s}$

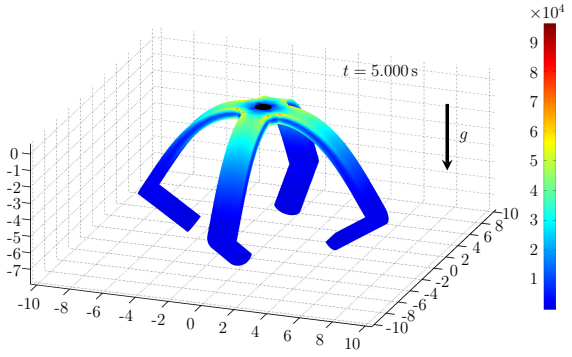

Figure 30: Actual configuration for the hyperelastic cantilever beam for the time $t = 5\,\mathrm{s}$

The balance of total linear momentum is for the variational integrator without a discrete gradient and with the VDG2 preserved. The same behavior is calculated for the balance of total angular momentum. For the calculation of the balance of total linear momentum we use Equation (48) and for the balance of total angular momentum we use once more Equation (50). However, before this we have to calculate the bearing forces with respect to Equation (62). The

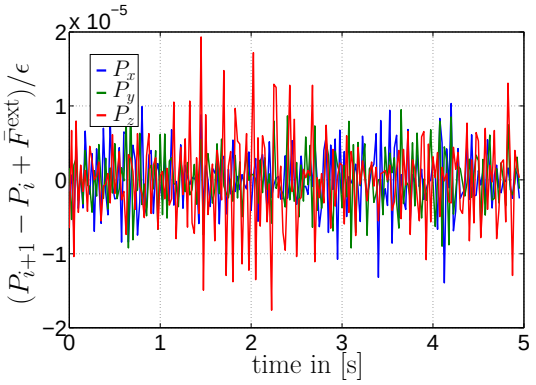

Figure 31: Balance of total linear momentum with VDG2 for hyperelastic cantilever beam with $n_{\text{p}} = 3$

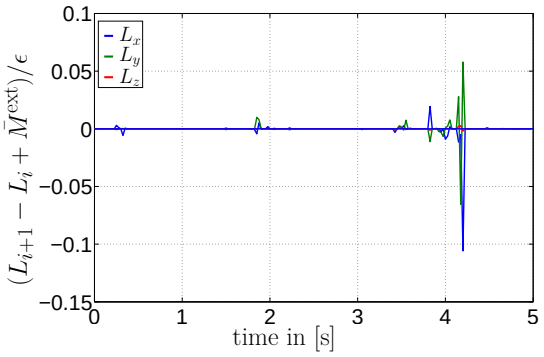

Figure 32: Balance of total angular momentum with VDG2 for hyperelastic cantilever beam with $n_{\text{p}} = 3$

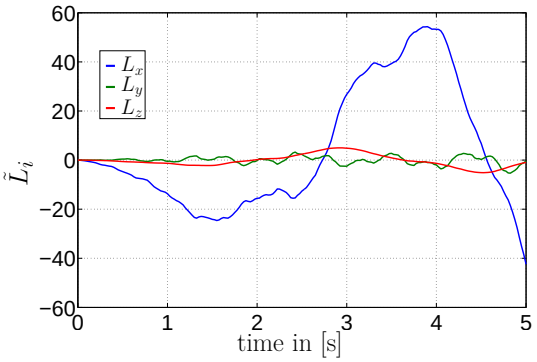

Figure 33: Angular momentum with VDG2 for hyperelastic cantilever beam with $n_{\text{p}} = 3$

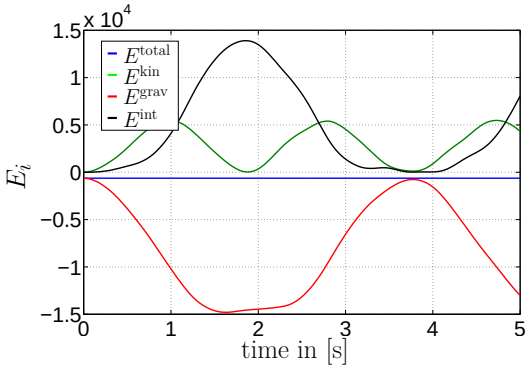

Figure 34: energy with VDG2 for hyperelastic cantilever beam with $n_{\text{p}} = 3$

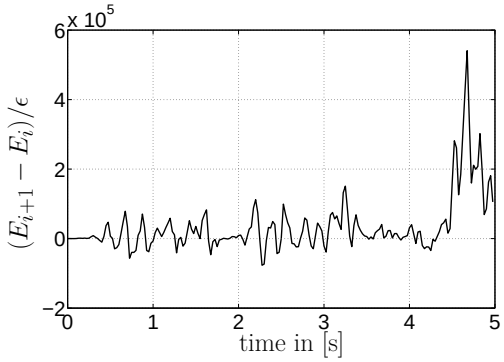

Figure 35: Balance of total energy without discrete gradient for hyperelastic cantilever beam with $n_{\text{p}} = 3$

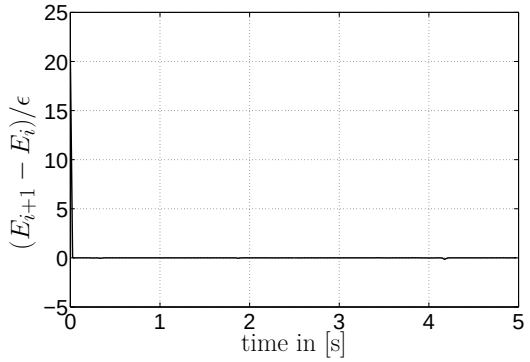

Figure 36: Balance of total energy with VDG2 for hyperelastic cantilever beam with $n_{\text{p}} = 3$

total angular momentum with the momentum term $\tilde{L}$ is printed in Figure 33. The values of the different energies over the simulation time are shown in Figure 34. Again, the variational integrator without a discrete gradient cannot preserve the balance of total energy, but the VDG2 is able to do it. In Figure 36 the complete balance is met for every time step, but not in the first

time step. Here the simulation starts in the first time step with a very small change in values for the strains. Therefore, for the time step scheme VDG2 it is difficult to handle elements which are nearly undeformed. This means that the NEWTON criterion will not be reached. This brings a little error in the balance of total energy for the first time step. For all the other time steps the balance of total energy is preserved.

5.4 VIBRATION OF HYPERELASTIC CANTILEVER BEAM WITH VDG1

The last numerical example is also the vibration of a cantilever beam. It is almost the same simulation as before, but now we want to use VDG1 time step scheme. We change the number of elements n_{el} to a smaller number and set a smaller time step size $h_n = 0.01\,\text{s}$, see Table 4.

n_{el}	560	n_{dof}	$3156 \cdot n_{\text{p}} = 9468$
h_n	$0.01\,\text{s}$	T_{end}	$5\,\text{s}$
n_{p}	3	ρ_0	8.93
$\rho_0\lambda$	$16.25 \cdot 10^4$	$\rho_0\mu$	$15 \cdot 10^6$
ϵ	$1 \cdot 10^{-7}$	$n_{\text{q,fix}}$	$72 \cdot n_{\text{p}} = 216$

Table 4: Simulation parameters for the vibration of the hyperelastic cantilever beam with VDG1

The reference configuartion is shown in the Figure 37. The single blades of the rotor also swing around their static equilibrium positions, but the vibration do not reach large values because the smaller number of elements makes the material more stiff.

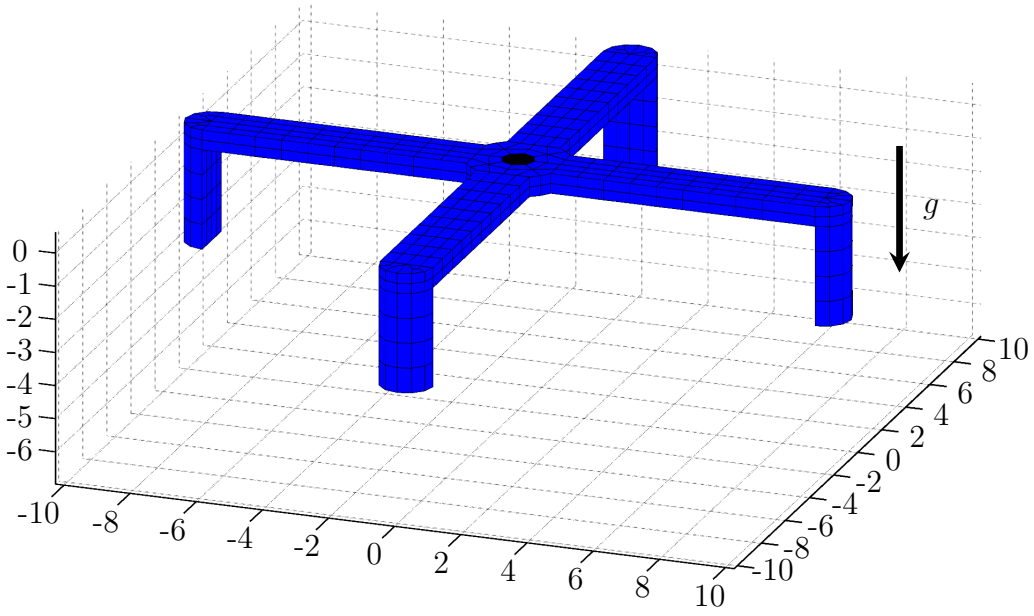

Figure 37: Reference configuration for the hyperelastic cantilever beam with VDG1 for the time $t = 0\,\text{s}$

This behavior can also be seen in the Figures 38-41 that show the vibration of the rotor for different time steps. The smaller values in the VON MISES stress can also be seen in the color bar at the right-hand side of every figure.

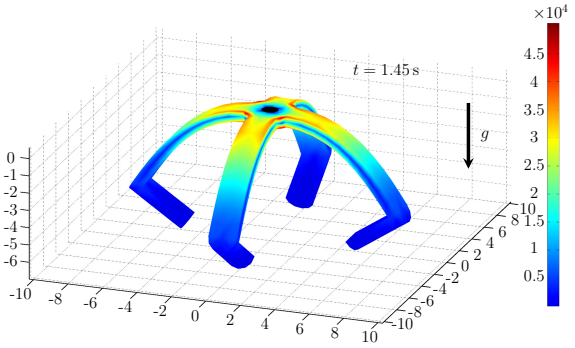

Figure 38: Actual configuration for the hyperelastic cantilever beam with VDG1 for the time $t = 1.45\,\mathrm{s}$

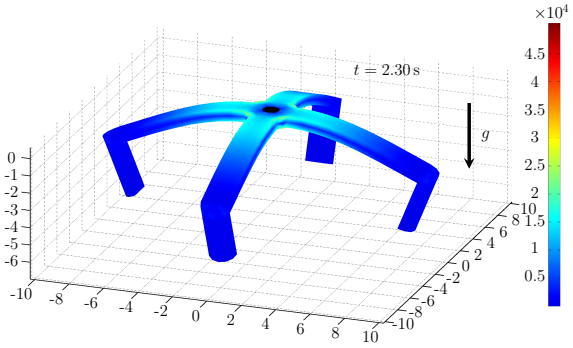

Figure 39: Actual configuration for the hyperelastic cantilever beam with VDG1 for the time $t = 2.3\,\mathrm{s}$

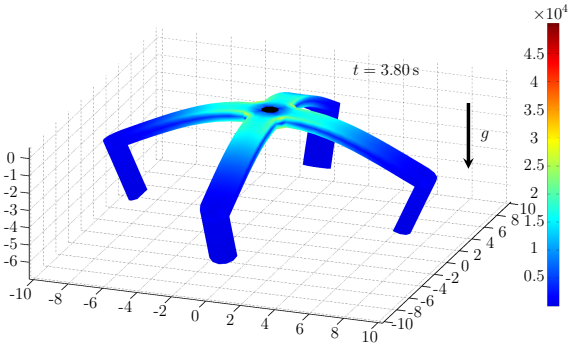

Figure 40: Actual configuration for the hyperelastic cantilever beam with VDG1 for the time $t = 3.8\,\mathrm{s}$

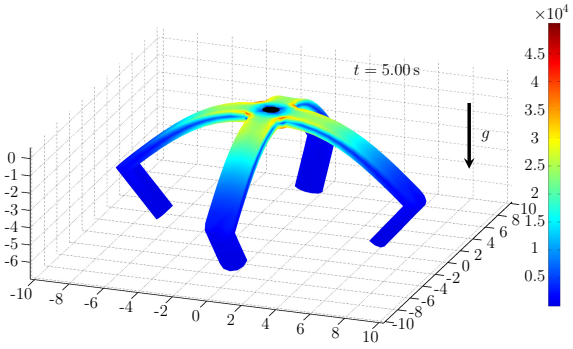

Figure 41: Actual configuration for the hyperelastic cantilever beam with VDG1 for the time $t = 5.0\,\mathrm{s}$

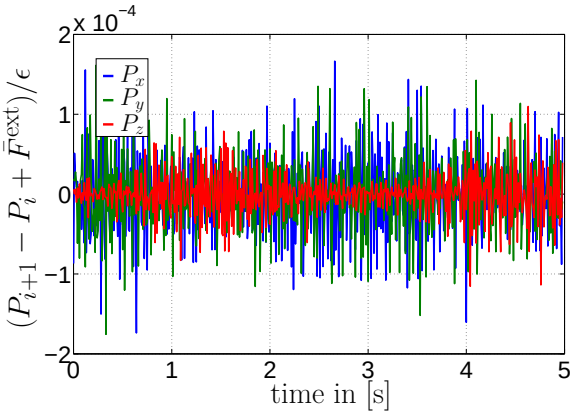

Figure 42: Balance of total linear momentum with VDG1 for hyperelastic cantilever beam with $n_\mathrm{p} = 3$

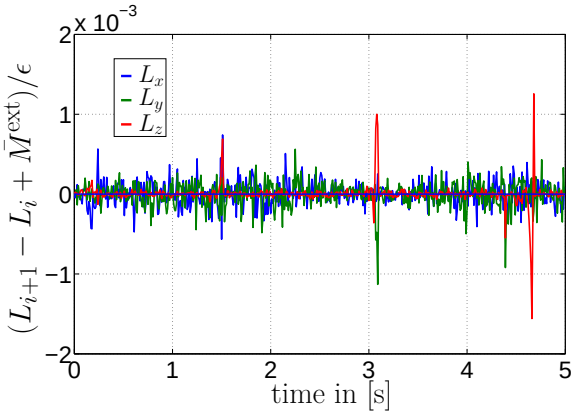

Figure 43: Balance of total angular momentum with VDG1 for hyperelastic cantilever beam with $n_\mathrm{p} = 3$

For these simulation parameters, the balance of total linear momentum and the balance of total angular momentum is met for every time step.
The Figures 44-45 show the different energies and the balance of the total total energy. Almost all values in the balance of total energy are preserved for all time steps. There is only a small number of peaks in which the balance is not met. This behavior can only be shown in the case of a very good choice of simulation parameters because the VDG1 method is numerically very instable, compare [4]. The simulation starts with normal results but, sometimes the NEWTON method cannot find a solution that fulfills the NEWTON criterion for the residual. In this case, the simulation finishes the time step with incorrect values. If this happened too often within the simulation, the entire simulation would diverge.

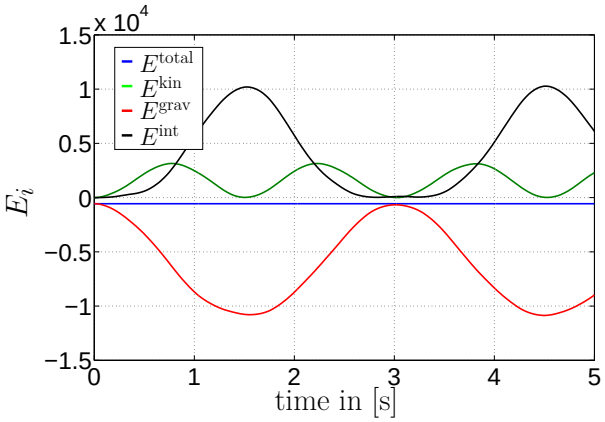

Figure 44: Energy with VDG1 for hyperelastic cantilever beam with $n_{\text{p}} = 3$

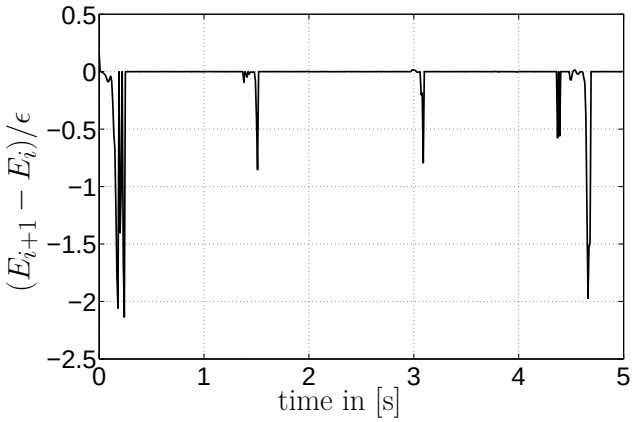

Figure 45: Balance of total energy with VDG1 for hyperelastic cantilever beam with $n_{\text{p}} = 3$

6 CONCLUSION

We have shown how a variational integrator of higher order accuracy can be consistently formulated for a hyperelastic continuum, and that this integrator meets the balance of total linear momentum and total angular momentum. The order of accuracy in position and momentum reaches the theoretical values if using the GAUSSIAN quadrature rule for the approximation of the position vector.
The inclusion of a LAGRANGE multiplier vector is also possible in the variational principle. The application of the NEWTON-COTÊS quadrature allows to decouple the equations in the position-momentum form. We have also shown how the bearing forces can be calculated from the LAGRANGE multiplier vector for the fixed nodes.
The split of the discrete gradient into two terms one in the LAGRANGIAN and one in a D'ALEMBERT term makes it also possible to create an integrator which meets the balance of total energy for every time step in the simulation. It is true that the integrator loses the symplecticity, but achieves the importanted total energy conservation for continuum problems.
However, it should be noted that an approximation of the right CAUCHY-GREEN tensor $\mathbf{C}$ with the position vector $\mathbf{q}$ is numerically instable, see VDG1. But, with an assumed strain approximation in the discrete gradient, the instabilities can be solved.
Further, the ongoing development of the computer hardware opens new possiblities for numerical simulations, like the parallelization of element routines on graphic cards with CUDA. That can save a lot of CPU time and makes time step schemes with better physical properties more attractive for further application.

ACKNOWLEDGEMENTS

The authors thank the 'Deutsche Forschungsgesellschaft (DFG)' for financial support of this work under the grant GR 3297/2-2 and Oliver Klöckner for his contribution about the parallelization of element routines with CUDA.

REFERENCES

[1] M. Groß, P. Betsch, P. Steinmann, Conservation properties of a time FE method. Part IV: Higher order energy and momentum conserving schemes. *Int. J. Numer. Meth. Engng* **63**, 1849–1897, 2005.

[2] P. Betsch, P. Steinmann, Conservation properties of a time FE method–part III: Mechanical systems with holonomic constraints. *Int. J. Numer. Meth. Engng.*, **53**, 2271–2304, 2002.

[3] P. Wriggers, *Nichtlineare Finite-Element-Methoden*, 1th Edition, Springer, Berlin, 2008.

[4] R. Mohr, *Consistent Time-Integration of Finite Elasto-Plasto-Dynamics*. Dissertation, 2008.

[5] M. Krüger, M. Groß, P. Betsch, An energy-entropy-consistent time stepping scheme for nonlinear thermo-viscoelastic continua. *ZAMM*, **96**, 141–178, 2016.

[6] S. Ober-blöbaum, N. Saake, Construction and analysis of higher order Galerkin variational integrators. *Advances in Computational Mathematics*, 1–32, 2014.

[7] J. E. Marsden and M. West, Discrete mechanics and variational integrators. *Acta Numerica*, **10**, 357–514, 2001.

[8] O. Gonzalez, Exact energy and momentum conserving algorithms for general models in nonlinear elasticity. *Computer Methods in Applied Mechanics and Engineering*, **190**, 1763–1783, 2000.

[9] M. Bartelt, M. Groß, Variational integrators of higher order for flexible multibody systems. *Proc. Appl. Math. Mech.*, **15**, 43–44, 2015.

[10] S. Hartmann, P. Ne, Polyconvexity of generalized polynomial-type hyperelastic strain energy functions for near-incompressibility. *International Journal of Solids and Structures*, **40**, 2767–2791, 2003.

[11] Nijmeyer H. and van der Schaft A.J., *Nonlinear Dynamical Control Systems*, Springer, New York, 1990.

A SHAPE FUNCTIONS IN TIME

The following matricies are time shape functions for the GAUSSIAN quadrature $\mathbf{M}_\mathrm{g}$ and for the NEWTON-COTÊS quadrature $\mathbf{M}_\mathrm{c}$. $\bar{\mathbf{M}}_\mathrm{g}$ and $\bar{\mathbf{M}}_\mathrm{c}$ are the shape functions one polynomial degree lower but with same quadrature points. $\mathbf{w}_\mathrm{g}$ and $\mathbf{w}_\mathrm{c}$ are the weights of the quadrature rule and $\boldsymbol{\alpha}_\mathrm{g}$ and $\boldsymbol{\alpha}_\mathrm{c}$ are the quadrature points.

$$\mathbf{M}_\mathrm{c} = \begin{bmatrix} M_{\mathrm{c}1,1} & M_{\mathrm{c}1,2} & \dots M_{\mathrm{c}1,n_\mathrm{c}+1} \\ M_{\mathrm{c}2,1} & M_{\mathrm{c}2,2} & \dots M_{\mathrm{c}2,n_\mathrm{c}+1} \\ \vdots & \vdots & \vdots \\ M_{\mathrm{c}n_\mathrm{c}+1,1} & M_{\mathrm{c}n_\mathrm{c}+1,2} & \dots M_{\mathrm{c}n_\mathrm{c}+1,n_\mathrm{c}+1} \end{bmatrix} \quad \bar{\mathbf{M}}_\mathrm{c} = \begin{bmatrix} \bar{M}_{\mathrm{c}1,1} & \bar{M}_{\mathrm{c}1,2} & \dots \bar{M}_{\mathrm{c}1,n_\mathrm{c}+1} \\ \bar{M}_{\mathrm{c}2,1} & \bar{M}_{\mathrm{c}2,2} & \dots \bar{M}_{\mathrm{c}2,n_\mathrm{c}+1} \\ \vdots & \vdots & \vdots \\ \bar{M}_{\mathrm{c}n_\mathrm{c},1} & \bar{M}_{\mathrm{c}n_\mathrm{c},2} & \dots \bar{M}_{\mathrm{c}n_\mathrm{c},n_\mathrm{c}+1} \end{bmatrix}$$

$$\mathbf{M}_\mathrm{g} = \begin{bmatrix} M_{\mathrm{g}1,1} & M_{\mathrm{g}1,2} & \dots M_{\mathrm{g}1,n_\mathrm{q}+1} \\ M_{\mathrm{g}2,1} & M_{\mathrm{g}2,2} & \dots M_{\mathrm{g}2,n_\mathrm{q}+1} \\ \vdots & \vdots & \vdots \\ M_{\mathrm{g}n_\mathrm{q},1} & M_{\mathrm{g}n_\mathrm{q},2} & \dots M_{\mathrm{g}n_\mathrm{q},n_\mathrm{q}+1} \end{bmatrix} \quad \bar{\mathbf{M}}_\mathrm{g} = \begin{bmatrix} \bar{M}_{\mathrm{g}1,1} & \bar{M}_{\mathrm{g}1,2} & \dots \bar{M}_{\mathrm{g}1,n_\mathrm{q}} \\ \bar{M}_{\mathrm{g}2,1} & \bar{M}_{\mathrm{g}2,2} & \dots \bar{M}_{\mathrm{g}2,n_\mathrm{q}} \\ \vdots & \vdots & \vdots \\ \bar{M}_{\mathrm{g}n_\mathrm{q},1} & \bar{M}_{\mathrm{g}n_\mathrm{q},2} & \dots \bar{M}_{\mathrm{g}n_\mathrm{q},n_\mathrm{q}} \end{bmatrix}$$

$$\mathbf{M}_\mathrm{g}^1 = \begin{bmatrix} M_{\mathrm{g}1,1} \\ M_{\mathrm{g}2,1} \\ \vdots \\ M_{\mathrm{g}n_\mathrm{q},1} \end{bmatrix} \quad \mathbf{M}_\mathrm{g}^\mathrm{n} = \begin{bmatrix} M_{\mathrm{g}1,2} & \dots M_{\mathrm{g}1,n_\mathrm{q}+1} \\ M_{\mathrm{g}2,2} & \dots M_{\mathrm{g}2,n_\mathrm{q}+1} \\ \vdots & \vdots \\ M_{\mathrm{g}n_\mathrm{q},2} & \dots M_{\mathrm{g}n_\mathrm{q},n_\mathrm{q}+1} \end{bmatrix}$$

$$\mathbf{w}_\mathrm{c} = \begin{bmatrix} w_{c_1} & 0 & \dots 0 \\ 0 & w_{c_2} & \dots 0 \\ \vdots & \vdots & \vdots \\ 0 & 0 & \dots w_{c_{n_\mathrm{q}+1}} \end{bmatrix} \quad \mathbf{w}_\mathrm{g} = \begin{bmatrix} w_{g_1} & 0 & \dots 0 \\ 0 & w_{g_2} & \dots 0 \\ \vdots & \vdots & \vdots \\ 0 & 0 & \dots w_{g_{n_\mathrm{q}}} \end{bmatrix}$$

$n_\mathrm{p} = 1$

$$\mathbf{M}_\mathrm{c} = \begin{bmatrix} 1 & 0 \\ 0 & 1 \end{bmatrix} \quad \bar{\mathbf{M}}_\mathrm{c} = \begin{bmatrix} 1 & 1 \end{bmatrix} \quad \mathbf{M}_\mathrm{g} = \begin{bmatrix} 0.5 & 0.5 \end{bmatrix} \quad \bar{\mathbf{M}}_\mathrm{g} = \begin{bmatrix} 1 \end{bmatrix}$$

$$\mathbf{w}_\mathrm{g} = \begin{bmatrix} 1 \end{bmatrix} \quad \mathbf{w}_\mathrm{c} = \begin{bmatrix} 0.5 & 0 \\ 0 & 0.5 \end{bmatrix} \quad \boldsymbol{\alpha}_\mathrm{g} = \begin{bmatrix} 0.5 \end{bmatrix} \quad \boldsymbol{\alpha}_\mathrm{c} = \begin{bmatrix} 0 & 1 \end{bmatrix}$$

$n_\mathrm{p} = 2$

$$\mathbf{M}_\mathrm{c} = \begin{bmatrix} 1 & 0 & 0 \\ 0 & 1 & 0 \\ 0 & 0 & 1 \end{bmatrix} \quad \bar{\mathbf{M}}_\mathrm{c} = \begin{bmatrix} 1 & 0.5 & 0 \\ 0 & 0.5 & 1 \end{bmatrix}$$

$$\mathbf{M}_\mathrm{g} \approx \begin{bmatrix} 0.4553 & 0.6666 & -0.1220 \\ -0.1220 & 0.6666 & 0.4553 \end{bmatrix} \quad \bar{\mathbf{M}}_\mathrm{g} \approx \begin{bmatrix} 0.7887 & 0.2113 \\ 0.2113 & 0.7887 \end{bmatrix}$$

$$\mathbf{w}_\mathrm{g} = \begin{bmatrix} 0.5 & 0.5 \end{bmatrix} \quad \mathbf{w}_\mathrm{c} \approx \begin{bmatrix} 0.1666 & 0 & 0 \\ 0 & 0.6666 & 0 \\ 0 & 0 & 0.1666 \end{bmatrix}$$

$$\boldsymbol{\alpha}_\mathrm{g} \approx \begin{bmatrix} 0.2113 & 0.7887 \end{bmatrix} \quad \boldsymbol{\alpha}_\mathrm{c} = \begin{bmatrix} 0 & 0.5 & 1 \end{bmatrix}$$